Chapter-5

LC-MS based Phytochemical Investigation Combined Network Pharmacology to Evaluate the Cytotoxic Potential of *A. cunninghamii* Mudie: Leaves

5 LC-MS-based Phytochemical Investigation Combined Network Pharmacology to Evaluate the Cytotoxic Potential of *A. cunninghamii* Leaves

5.1 Introduction

The tall, evergreen coniferous tree *A. cunninghamii* (*Araucariaceae*), also referred to as Hoop pine, commonly grows to a height of over 20 m. Asia, it is widely distributed in the Himalayan regions of Pakistan and India [157]. It is a native species to northeastern Australia growing widely in the subtropical vine forests [158] and it is abundantly grown for timber production in this region. It is also used in some rituals by the people of New Guinea and its bark is used for that ching purposes [159]. Numerous phytoconstituents, primarily diterpenes and biflavones, have been identified from various species of *Araucaria*. Phytochemical studies on different parts of the plant have revealed that *A. cunninghamii* gum-resin is a rich source of labdane and abietane diterpenoids [119]. Aerial parts, particularly leaves, are considered non-edible and toxic. This toxicity may be attributed to the several biflavones such as amentoflavone [160], agathisflavones [161], cupresuflavones [162], robustaflavones [163], and hinokiflavones [164]. These biflavones have been reported from the different species of the genus Araucaria. Biflavones are an important class of phenolic metabolites possessing a wide range of biological activities [165]. They have been explored for anti-microbial [166], antiviral [167], anti-ulcerogenic [168], cytotoxic [169], antineoplastic [170], mutagenic [171], antioxidant [172], antihepatotoxic [173], antihypertensive

[174, 175], hypolipidemia [176], anti-platelet [177], and anti-inflammatory activities [119, 178]

In the quest for the search of potential anticancer leads from *A. Cunninghamii*, our previous report disclosed the isolation of novel labdane diterpenoids from the gum resin [119]. This work is focused on the phytochemical investigation of leaves. The current work focuses on non-targeted chemo profiling by LC-HRMS, followed by precise identification of metabolites by databases mining in the Dictionary of Natural Products (DNP). Identified metabolites were subjected to purification as well as to network pharmacological approaches to find probable gene targets and mechanisms, elucidating their therapeutic potential. Furthermore, the cytotoxic activity of the isolated compounds was assessed against the human gastric cancer cell line (AGS cell line). Additionally, the identified compounds were subjected to molecular docking with identified targets (PI3KR1, EGFR, and GSK3B) to analyse binding affinities.

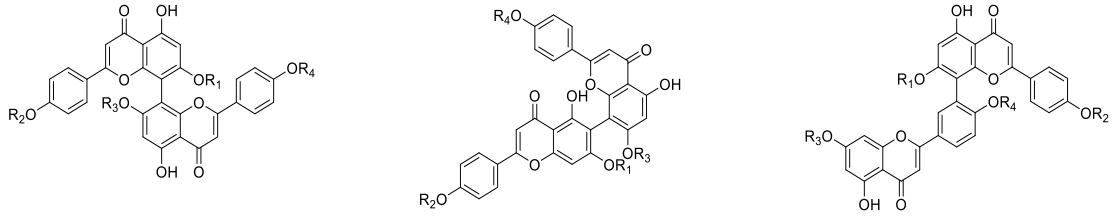

Cupressuflavone (R_1=R_2=R_3=R_4= H) (**AC8**)
4',4''',7,7''-tetra-Me-ether (R_1=R_2=R_3=R_4= CH_3): WB_1(**AC1**)
4',7,7''-tri-Me-ether (R_1=R_2=R_3: CH_3, R_4= H)
7',7''-di-Me ether (R_1=R_3: CH_3, R_2=R_4= H): (**AC2**)
4',4'''-di-Me-ether (R_2=R_4= CH_3, R_1=R_3= H): W_{11} (**AC5**)
4'-Me-ether (R_1=R_3=R_4= H, R_2= CH_3)

Agathisflaone (R_1=R_2=R_3=R_4= H)
4',4''',7,7''-tetra-Me-ether (R_1=R_2=R_3=R_4= CH_3) (**AC7**)
4''',7,7''-tri-Me-ether (R_1=R_2=R_3= CH_3, R_4= H) (**AC6**)
7,7''-di-Me-ether (R_1=R_3= CH_3, R_2=R_4= H)
7-Me-ether (R_1= CH_3, R_2=R_3=R_4= H)

Ametoflavone (R_1=R_2=R_3=R_4= H)
4',4''',7,7''-tetra-Me-ether (R_1=R_2=R_3=R_4= CH_3)
7,7''-Di-Me ether (R_1=R_3= CH_3, R_2=R_4= H)
7-Me-ether (R_1= CH_3, R_2=R_3=R_4= H)

Figure 5. 1 Chemical structures of the common biflavones from *A. cunninghamii* leaves

These biflavones are dimers of apigenin and the chemical diversity generated by linking two units of apigenin. These biflavones are mainly fall under three major isomeric categories based on the linking of both flavone moieties; cupressuflavone (8-8’ linking) [179], agathisflavones (6-8’ link) [180] and amentoflavones (8-3’ link) [181] as shown

below. Variety of methoxy substitutions, generated diverse and structurally related isomeric metabolites.

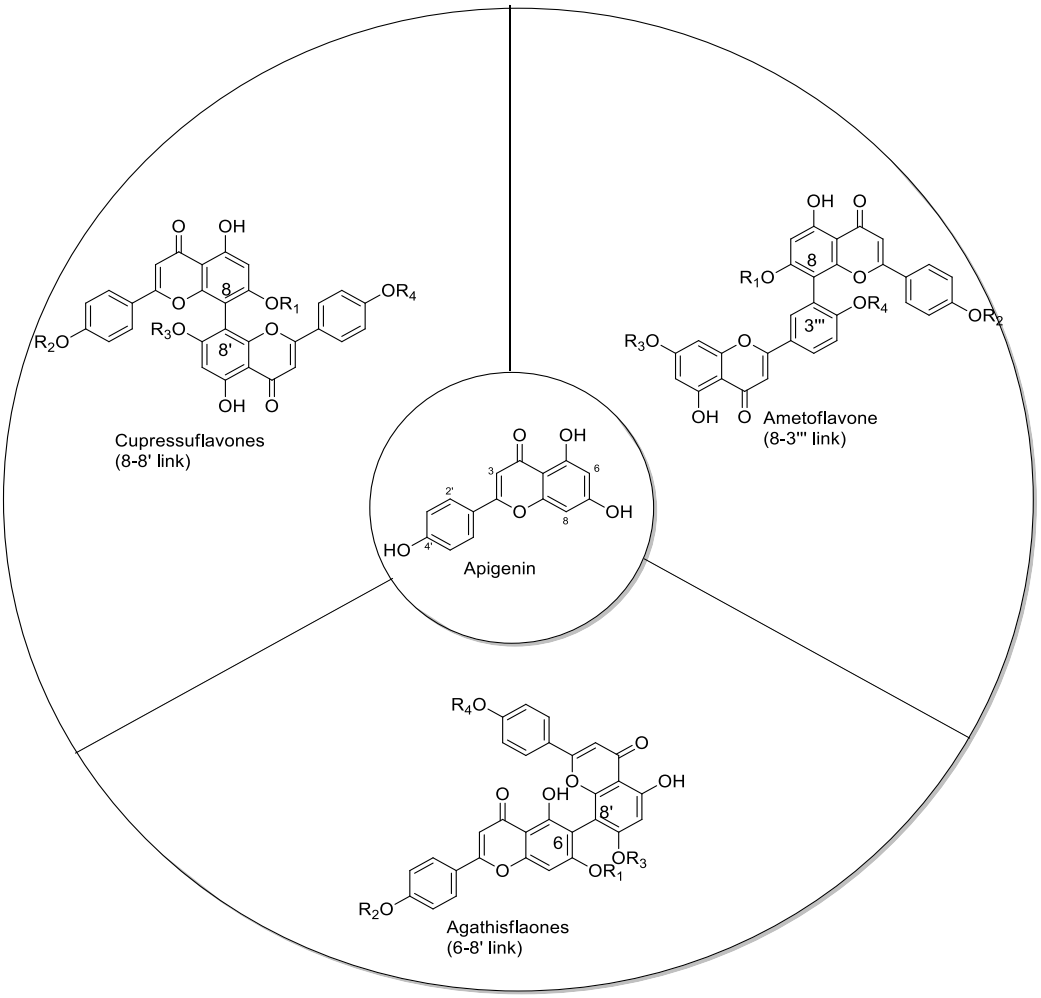

Figure 5. 2 Chemistry of biflavones

5.1.1 SAR of biflavones

The SAR (Structure-Activity Relationship) of biflavones, like many natural products, involves understanding how their chemical structure relates to their biological activity. Biflavones are dimeric flavonoids composed of two flavone units linked together [182].

Here are some key points in their SAR:

Linkage Type: The way in which the two flavone units are connected (e.g., via C-C or C-O-C bonds) can significantly influence their biological activity. Different linkages can alter their stability, solubility, and interaction with biological targets [183].

Substitution Pattern: The substitution pattern on the flavone units (hydroxyl groups, methoxy groups, etc.) affects their polarity, lipophilicity, and ability to interact with enzymes, receptors, or other biomolecules [184].

Ring Cleavage: Biflavones can undergo ring cleavage under certain conditions, leading to the formation of different metabolites that may have altered biological activities compared to the parent compound.

Stereochemistry: The spatial arrangement (stereochemistry) of atoms within the biflavone molecule can determine its interaction with chiral receptors or enzymes, influencing its biological effects [185].

Bioavailability: Factors such as molecular size, polarity, and ability to cross biological membranes (bioavailability) also play a crucial role in determining the overall biological activity of biflavones [186].

Target Specificity: Biflavones can exhibit selective activity against specific targets (enzymes, receptors, etc.) depending on their structural features, making understanding SAR important for drug design and development.

To delve deeper into the SAR of specific biflavones and their biological activities, detailed studies involving synthesis, structural modification, and bioassays are typically conducted. These efforts aim to optimize their pharmacological potential and

therapeutic applications

5.2 Results and discussion

5.2.1 Phytochemical investigation of *A. cunninghamii* leaves

The dried leaves of AC were dissolved in methanol, the soluble and insoluble portions were separated through filtering. After that, the soluble material was concentrated, and its cytotoxicity was assessed. The ethyl acetate fraction was concentrated for further phytochemical analysis after it was further fractionated using ethyl acetate-water partitioning. Simultaneously, the ethyl acetate fraction was subjected to LC-MS analysis and chromatographic purification through silica gel column chromatography, Sephadex LH-20, and Preparative TLC by using hexane-ethyl-acetate respectively.

Total eight compounds were isolated and characterised using 1D and 2D NMR spectroscopy and mass spectrometric analysis. Apart from that other known compound viz. cupressuflavone, agathisflavones, amentoflavones **(Figure 5.3)** were identified by comparing the observed NMR spectra with the reported spectroscopic data**.**

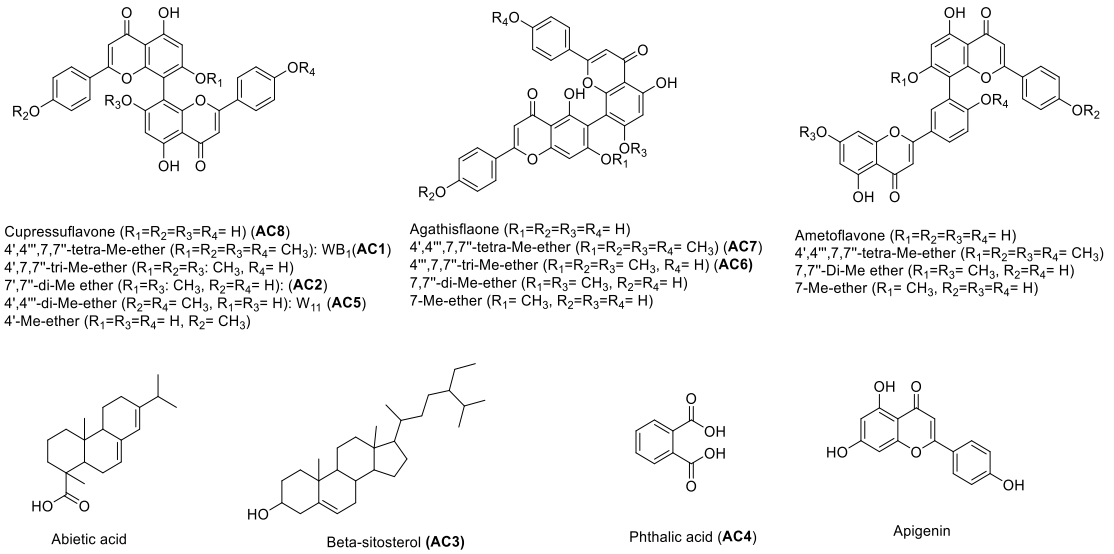

Figure 5.3 Chemical structure of compounds isolated (AC1 – AC8) from of *A. cunninghamii* leaves

5.2.2 Chromatographic separation and characterization of metabolites

For the isolation of targeted metabolites, fraction 2 (Eluted at 30% ethyl acetate in hexane, as described in experimental section) was loaded to LH20 Sephadex size exclusion column chromatography to obtain abundantly present abietic acid. Abietic acid was confirmed by co-TLC with authentic samples and by NMR. After purification of abietic acid, rest of the subfractions of fr-2 were pooled together and subjected to semi-prep HPLC for purification of the targeted molecules. Repeated purification by HPLC yielded compounds AC1– AC5. Extensive spectroscopic studies, including 2D NMR, were conducted to characterize these purified metabolites. These were characterized as cupresuflavone; 4′,4″,7,7″ tetra-methoxy or WB1(AC1), cupresuflavone; 7,7″-dimethoxy (AC2), beta-sitosterol (AC3), phthalic acid (AC4), and cupresuflavone; 4′,4″-dimethoxy or W11 (AC5). Interestingly cupressuflavone; 4′,7,7″-tri-methoxy (isomer of AC6, which is agathisflavone) was also obtained as a new metabolite from the *A. cunninghamii*, marking the first report of this previously undescribed compound. For the characterization of biflavone compounds, HRMS spectra of these compounds displayed $[M+H]^+$ peaks at m/z 595.1585, 567.1274, and 553.1111. Additionally, their ^{1}H-NMR spectra resembled those of flavonoids. Careful examination of the 1D and 2D NMR (^{1}H, ^{13}C, DEPT-135, ^{1}H-^{1}H COSY, HSQC, and HMBC experiments) spectra and comparison with existing literature led us to characterize these compounds as cupresuflavone; 4′,4″,7,7″ tetra-methoxy (AC1), cupresuflavone; 7,7″-dimethoxy (AC2), and cupresuflavone; 4′,4″-dimethoxy (AC5). The investigation also yielded two common metabolites β-sitosterol (AC3) and phthalic acid (AC4) that were confirmed by matching experimental NMR data with previously reported values [187]. The NMR spectra (page-66-71) are given below of AC1-AC2.

5.2.3 LC-HRMS and database mining for identification of metabolites

Air-dried leaves of *A. cunninghamii* were extracted using methanol, and the organic solvent was subsequently removed under vacuum. The resulting extract exhibited significant cytotoxic potential, with an IC_{50} value of 25 μg/mL. The extract was planned for phytochemical investigation for the isolation of bioactive secondary metabolites via bioassay-guided fractionation, combined with LC-HRMS analysis and strategic database mining. During the preparation of the extract, a crystalline substance was obtained while concentrating the methanolic extract. These crystals were directly separated by filtration and characterized as phthalic acid (AC4). The fraction 2 eluted at 30% ethyl acetate in hexane, as described in experimental section, has shown cytotoxicity (IC_{50}: 11μg/mL) against the ASG cells, taken for further isolation and characterization of the metabolites. Simultaneously, the active fraction was analyzed by LC-HRMS for identification of bioactive molecules **(Figure-5.4)**. LC-HRMS data revealed major ions with *m/z* (M+H): 303.2319, 553.1111, 567.1274, 581.1440, and 595.1578. The peak at *m/z* 303.2319 $(M+H)^+$, appearing at 12.1 min as major metabolite, was deduced to $C_{20}H_{30}O_2$ which is corresponding to abietic acid. Abietic acid has been isolated abundantly from this plant in our previous study, and its identity was also confirmed by an authentic sample available in our laboratory from the past study [119]. Rest of the ions with *m/z* $(M+H)^+$ 553.1111, 567.1274, 581.1440, and 595.1578 were deduced to $C_{31}H_{20}O_{10}+H^+$, $C_{32}H_{22}O_{10}+H^+$, $C_{33}H_{24}O_{10}+H^+$, and $C_{34}H_{26}O_{10}+H^+$ respectively,–appeared at different retention times.

As an observation, the molecular formula having carbon (C_{30}), can be assumed as triterpenoids, glycosides, or biflavones in general. The possibilities of tri-

terpenoids and glycosides were ruled out based on the number of hydrogen atoms in the molecular formula, which ranged from H_{20} to H_{26}. Typically, triterpenoids and glycosides have a higher number of hydrogen atoms ($>H_{40}$), leading to the assumption that the compounds were biflavones instead. These biflavones mainly fall into three major isomeric categories based on the linkage of both flavone moieties: cupressuflavone (8–8′ linking), agathisflavones (6–8′ link), and amentoflavones (8–3″ link), as shown in **(Fig-5.2)**. A variety of methoxy substitutions generated diverse and structurally related isomeric metabolites. Isomers cannot be distinguished by mass or molecular formula, hence by LC-HRMS data. So, all the assumed and reported structures were taken into consideration after the strategic database mining. After assuming presence of biflavones in the active fraction (fr-2), a systematic DNP-LC-PDA/MS-based strategic database mining approach was adopted for the precise identification of these metabolites. The DNP (available at https://dnp.chemnetbase.com/) is a comprehensive database of approximately 350,000 natural products. It has been explored systematically for the identification of known metabolites based on preliminary information and to target the known and new metabolites [104]. Further, the preliminary information like, biological sources, mass, molecular formula and UV spectrum were used as filters in DNP searches for precise results.

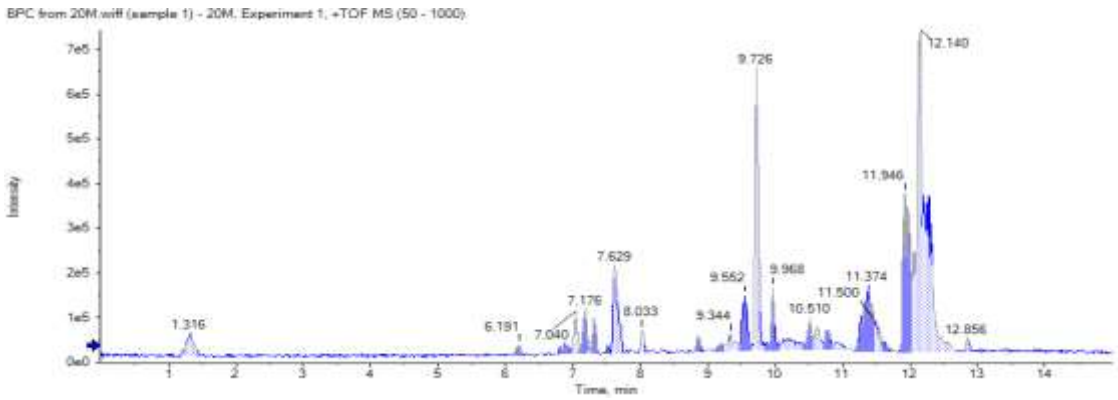

Figure 5.4 DNP LC-PDA/MS based strategic database mining approach used herein is described as follows

Toxic biflavones, such as amentoflavones, have been identified from the leaves of different species of *Araucaria.* DNP searches 19 biflavones from the genus and 5 from the species. For example, using m/z 553.1111 $(M+H)^+$ as a search query (accurate mass range: 552.000 to 552.999) within the species (Biological sources: *A. cunninghamii*) resulted in zero hits, while within the genus *Araucaria*, it yielded two hits. This suggests that the biflavone m/z 553.1111 $(M+H)^+$ is not reported in *A. cunninghamii*. Similarly, information were acquired for m/z $(M+H)^+$ 567.1274, 581.1440, and 595.1578 from DNP, as listed in. Simultaneously, the same extract was subjected to HPLC analysis, and the UV spectra of these metabolites were recorded on PDA. Using UV maxima 328 nm in DNP search in the genus *Araucaria* also resulted in biflavones. Thus, the DNP-LC-PDA/MS based strategic database mining precisely confirmed the presence of the biflavone metabolites in fr-2. The precise identification prompted us to isolate and characterize the biflavones.

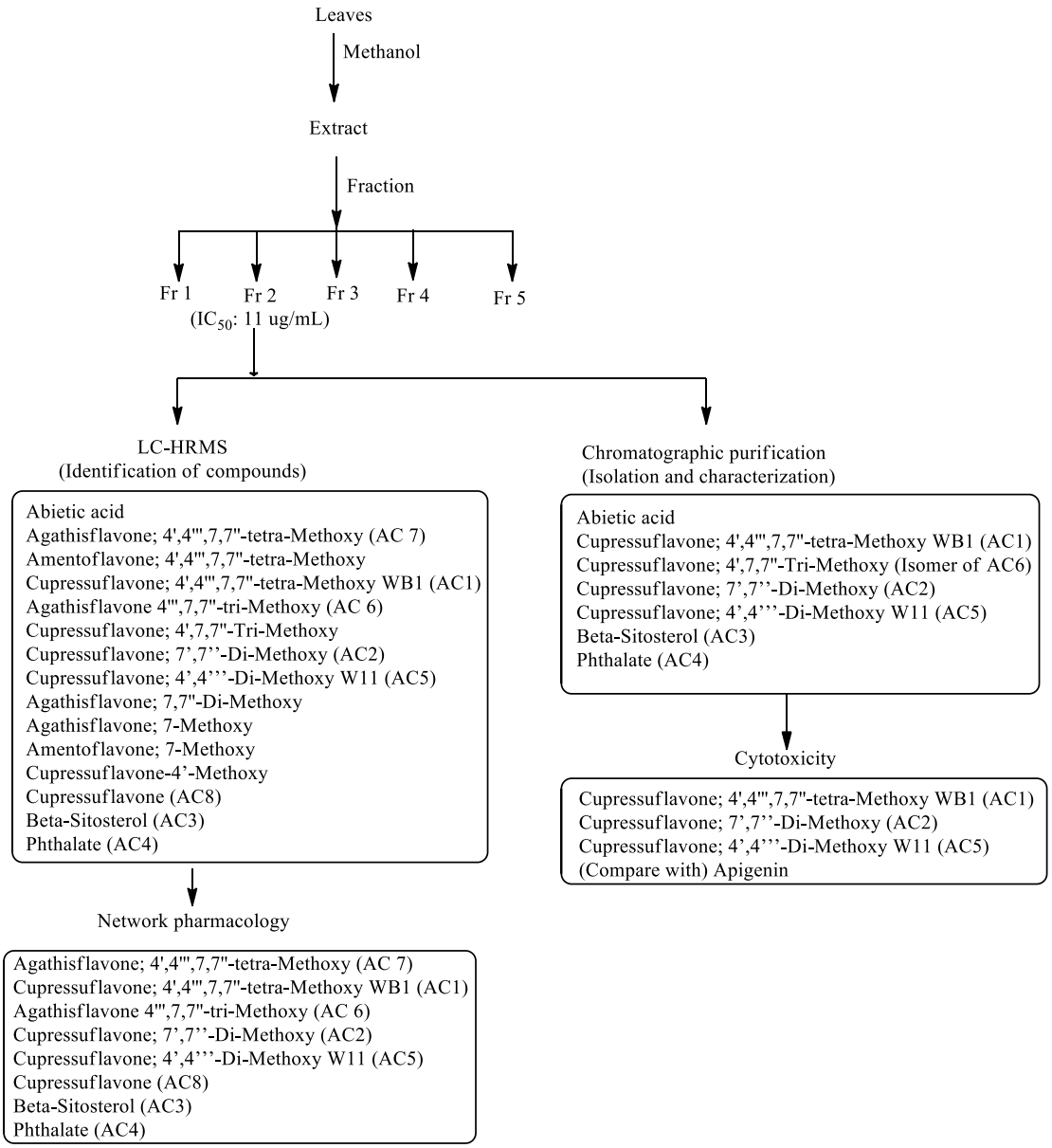

Figure 5. 5 Summary of extraction of compound from column chromatogram

Cupresuflavone-4',4''',7,7'' tetra-methoxy or WB1 (AC1)

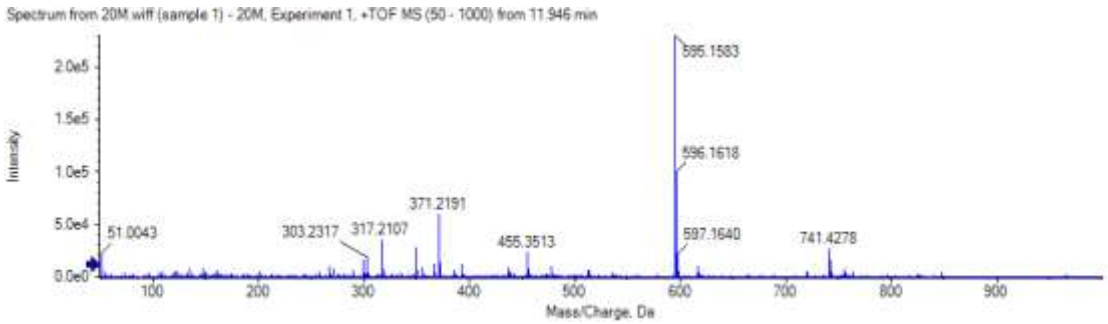

Figure 5. 6 Spectrum of Cupresuflavone-4',4''',7,7'' tetra-methoxy or WB1 (AC1)

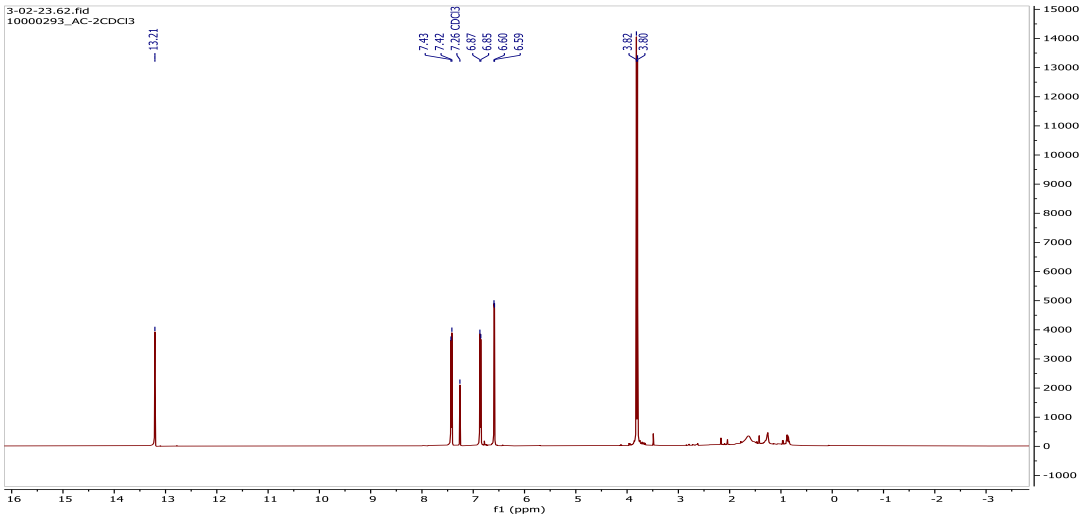

Figure 5. 7 ^{1}H-NMR (500 MHz; $CDCl_3$) spectrum of Cupresuflavone-4',4''',7,7'' tetra-methoxy or WB1 (AC1)

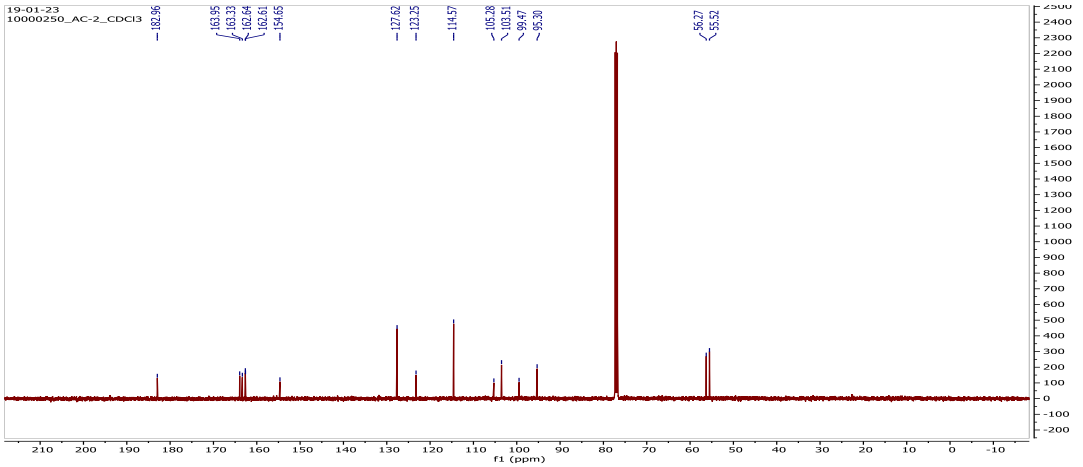

Figure 5. 8 ^{13}C-NMR (500 MHz; $CDCl_3$) spectrum of Cupresuflavone-4' 4''',7,7'' tetra-methoxy or WB1 (AC1)

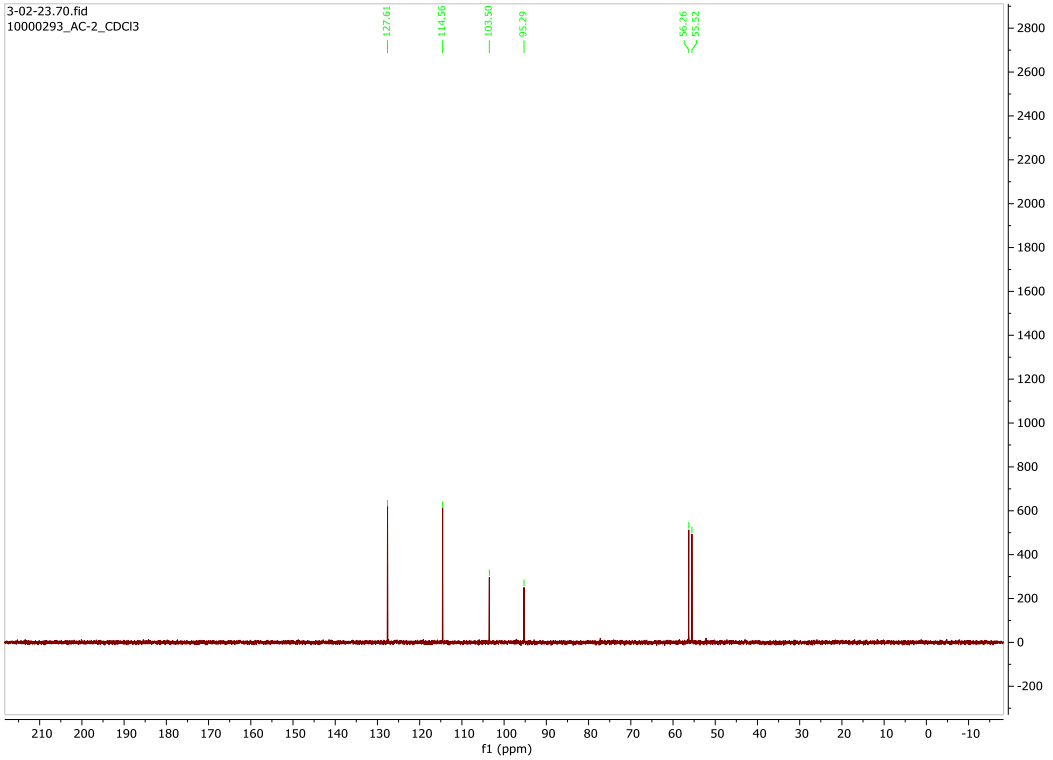

Figure 5. 9 DEPT-135 (500 MHz; $CDCl_3$) spectrum of cupresuflavone-4',4''',7,7'' tetra-methoxy or WB1 (AC1)

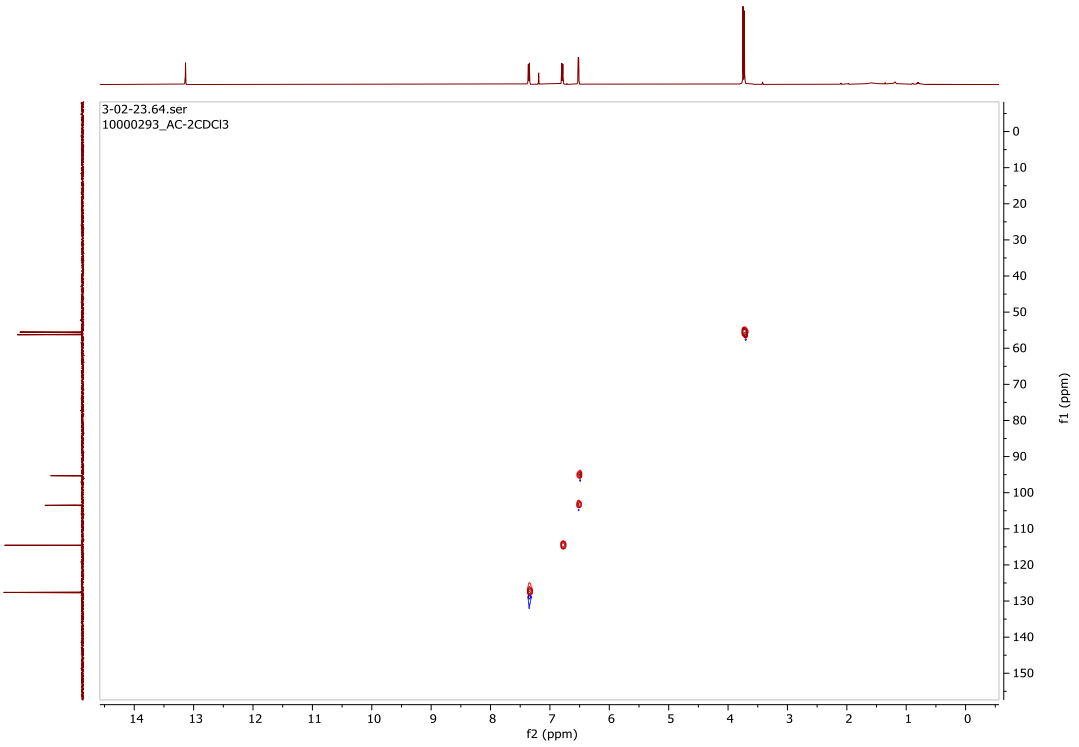

Figure 5. 10 HSQC (500 MH; $CDCl_3$) spectrum of cupresuflavone-4',4''',7,7'' tetra-methoxy or WB1 (AC1)

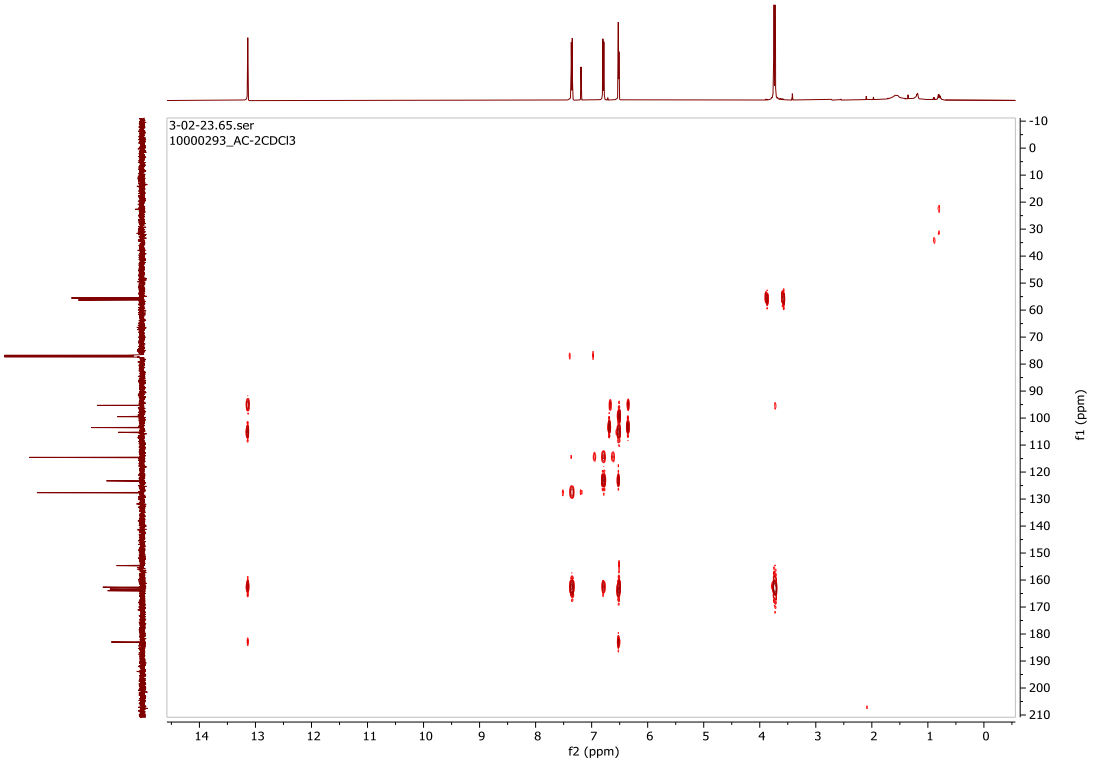

Figure 5. 11 HMBC (500 MHz; $CDCl_3$) spectrum of cupresuflavone-4',4''',7,7'' tetra-methoxy or WB1 (AC1)

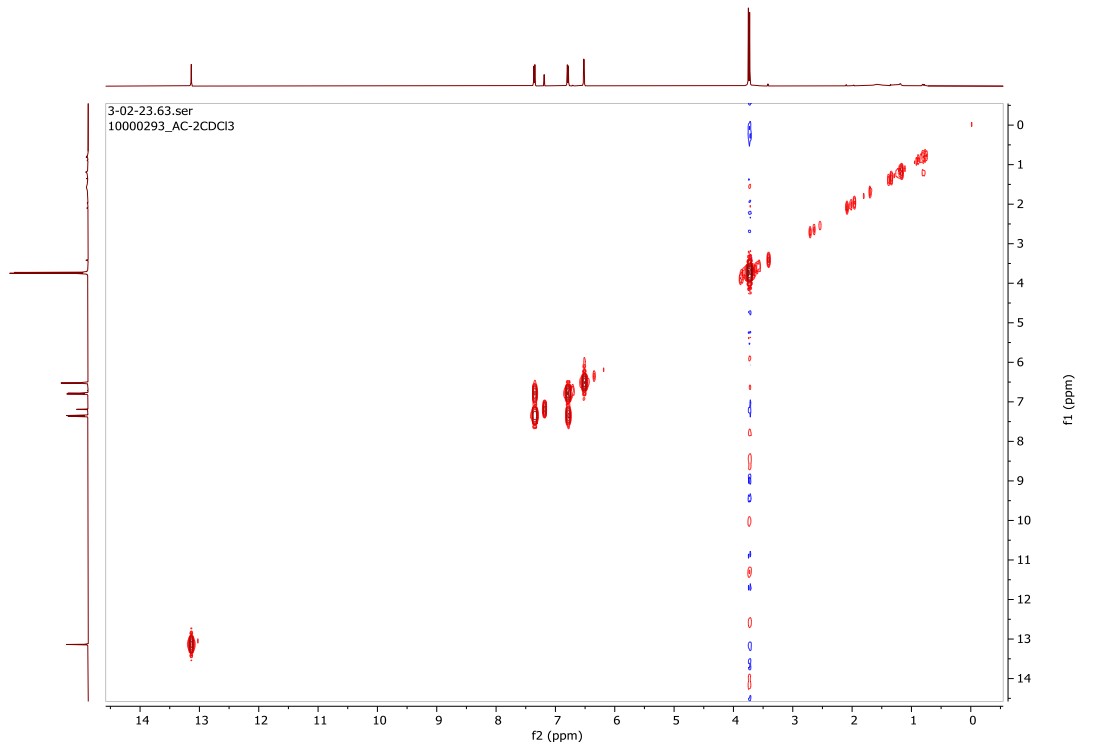

Figure 5. 12 COSY (500 MHz; $CDCl_3$) spectrum of cupresuflavone-4',4''',7,7'' tetra-methoxy or WB1 (AC1)

Cuppresuflavone-7,7''-dimethoxy (AC2)

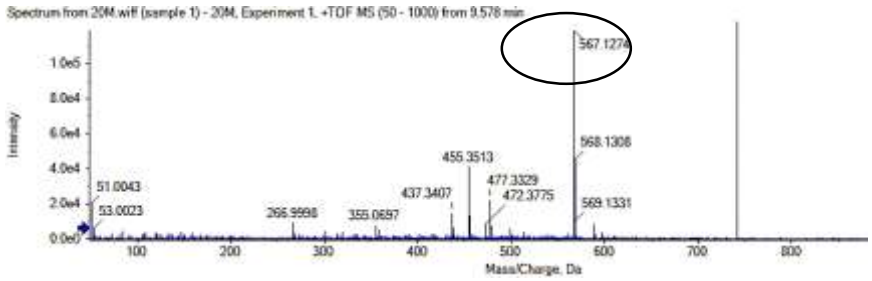

Figure 5. 13 Mass spectra of Cupressuflavone; 7',7''-Di-Me-ether (AC2)

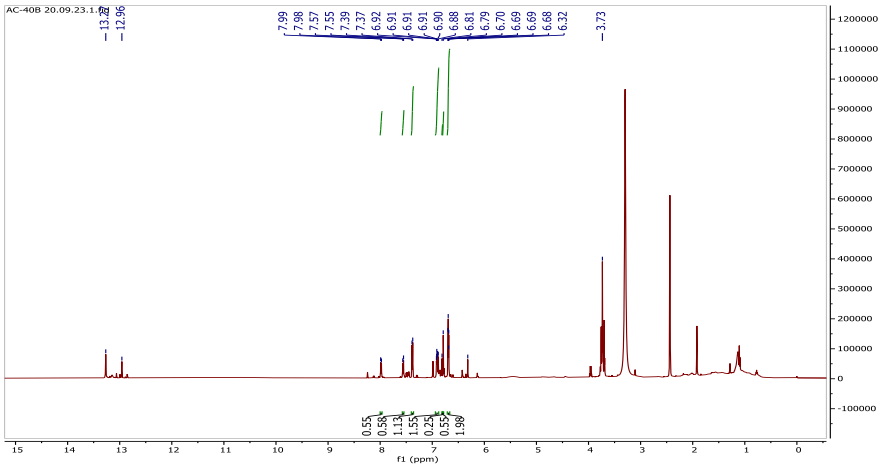

Figure 5. 14 ^{1}H-NMR (600 MHz; DMSO) spectrum of cuppresuflavone-7,7''-dimethoxy (AC2)

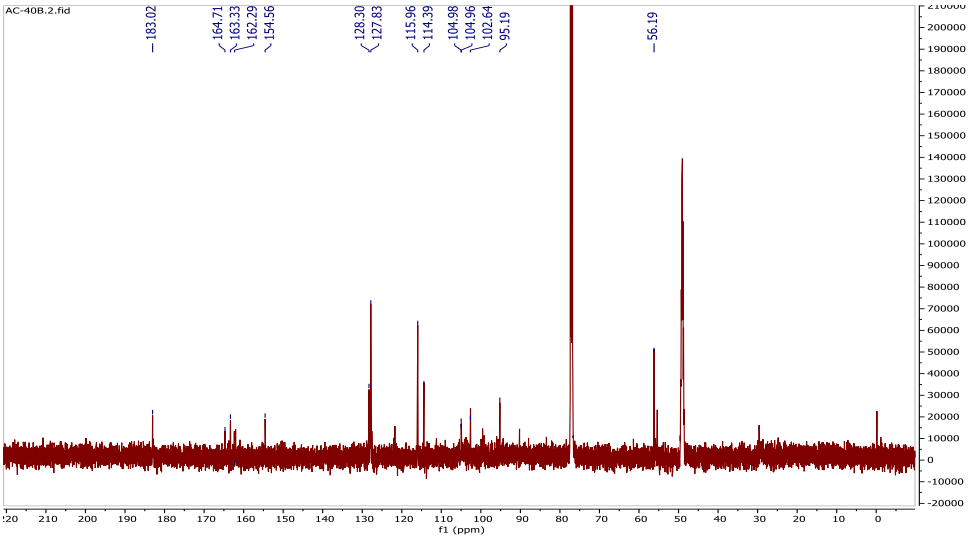

Figure 5. 15 ^{13}C-NMR (600 MHz; DMSO) spectrum of cuppresuflavone-7,7''-dimethoxy (AC2)

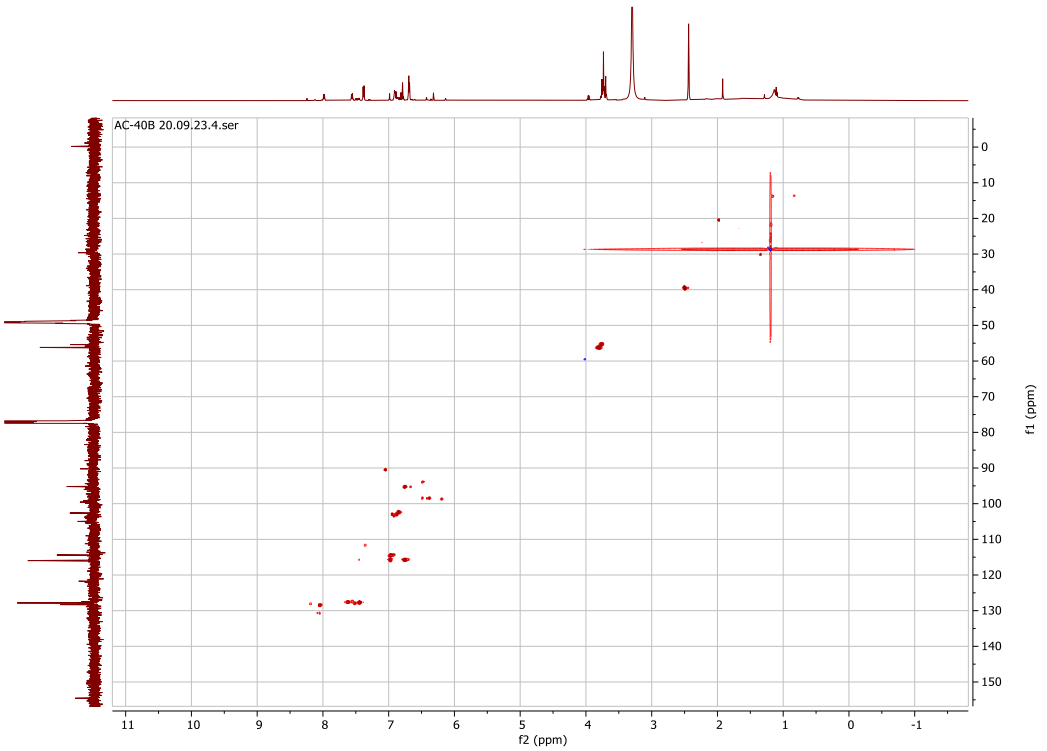

Figure 5. 16 HSQC (600 MHz; DMSO) spectrum of cuppresuflavone-7,7''-dimethoxy (AC2)

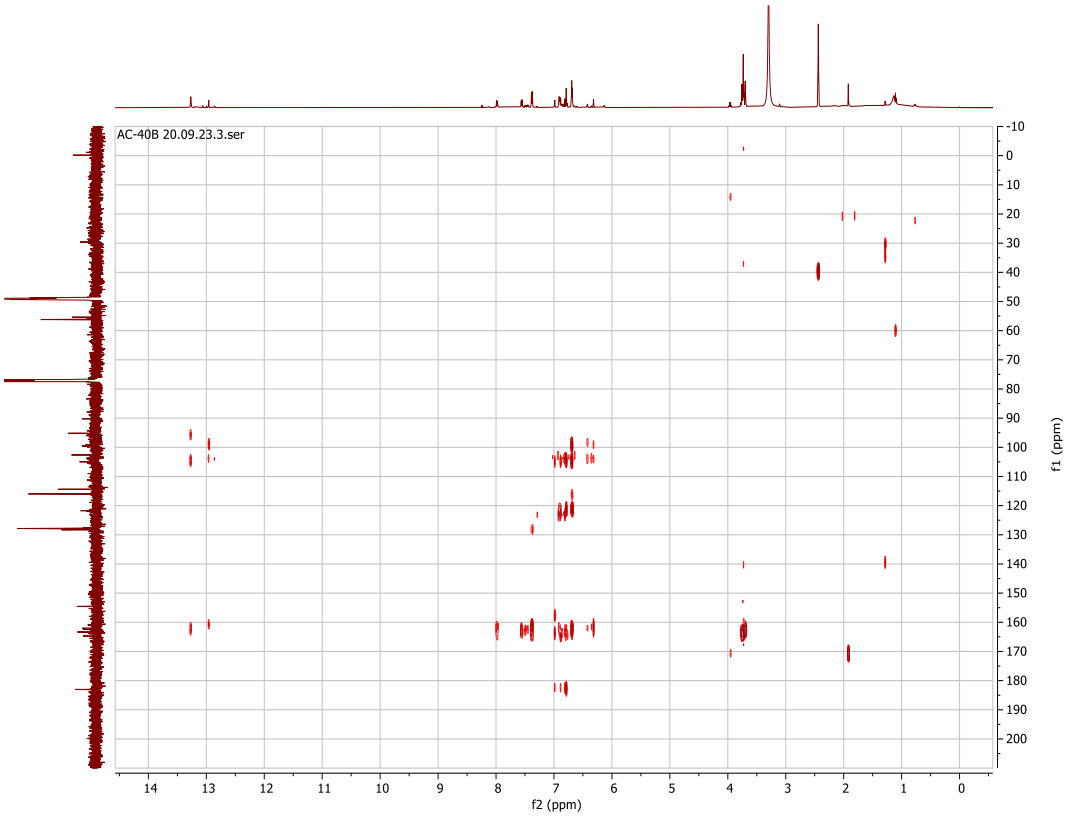

Figure 5. 17 HMBC (600 MHz; DMSO) spectrum of cuppresuflavone-7,7''-dimethoxy (AC2)

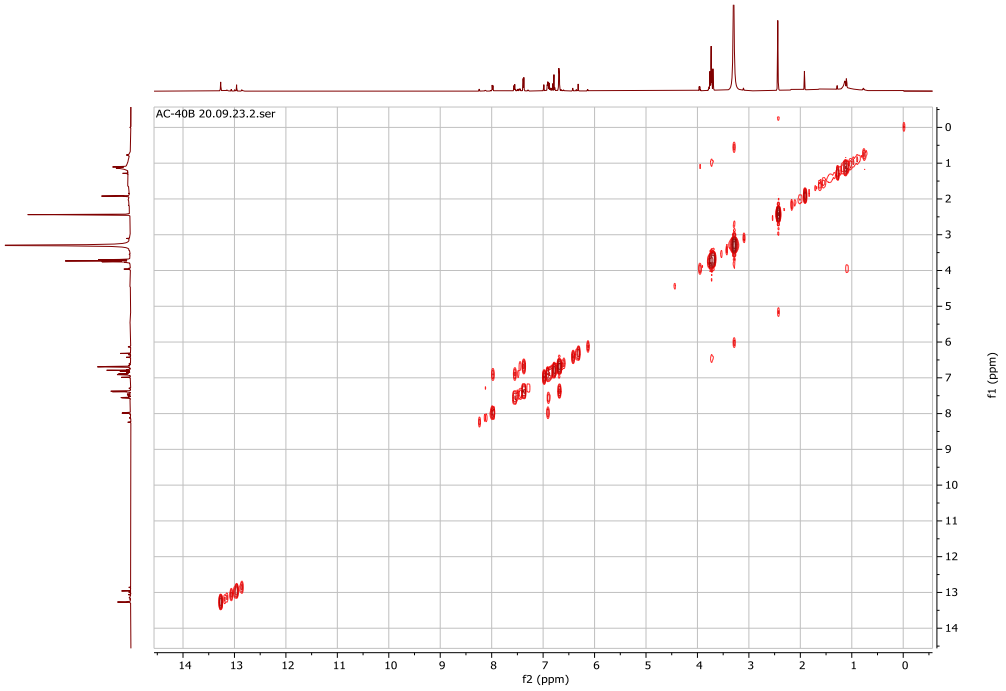

Figure 5. 18 COSY (600 MHz; DMSO) spectrum of cuppresuflavone-7,7''-dimethoxy (AC2)

Table 5. 1 Results of LC-HRMS profiling and database mining (AC1-AC8)

t_R (Min)	Observed *m/z* $[M+H]^+$	Cald m/z $[M+H]^+$	Chemical formula	Error, ppm	Identification
12.3	303.2319	303.2319	$C_{20}H_{30}O_2+H^+$	0	Abietic acid*
11.37-11.96	595.1585	595.1593	$C_{34}H_{26}O_{10}+H^+$	-1.34	Agathisflavone; 4',4'",7,7"-tetra-Methoxy (AC 7) Amentoflavone; 4',4'",7,7"-tetra-Methoxy Cupressuflavone; 4',4'",7,7"-tetra-Methoxy; WB1 (AC1)
10.5	581.1406	581.1430	$C_{33}H_{24}O_{10}+H^+$	-4.12	Agathisflavone 4'",7,7"-tri-Methoxy (AC 6) Cupressuflavone; 4',7,7"-tri-Methoxy
9.34-9.96	567.1274	567.1280	$C_{32}H_{22}O_{10}+H^+$	-1.05	Cupressuflavone; 7',7''-Di- Methoxy (AC2) Cupressuflavone; 4',4'''-Di- Methoxy; W11 (AC5) Agathisflavone; 7,7"-Di- Methoxy
8.86 7.10 7.6	553.1111	553.1124	$C_{31}H_{20}O_{10}+H^+$	-2.3	Agathisflavone; 7-Methoxy Amentoflavone; 7-Methoxy Cupressuflavone-4'-Methoxy
6.1	539.0972	539.0978	$C_{30}H_{18}O_{10}+H^+$	1.112	Cupressuflavone (AC8)
6.6	415.2296	414.3934	$C_{29}H_{50}O+H^+$		*β*-Sitosterol (AC3)*

From the identified compounds, only 8 of them were shortlisted for the network pharmacology studies and given the codes AC1 to AC8. The compounds were shortlisted based on their reports in PubChem, with inclusion criteria – *Araucaria*. Crystalline substance obtained during the extract preparation was characterized as phthalic acid (AC6)
*Confirmed by co-TLC with authentic sample available in our laboratory

5.2.4 Virtual ADME screening of compound

Eight compounds were selected for network pharmacology analysis based on literature survey. Compound AC8 was rejected in this virtual ADME study as it violates more

than one Lipinski's rule, whereas compounds AC1–AC7 were accepted. Compounds were mostly found to possess favourable pharmacokinetic properties like bioavailability, human intestinal absorption (HIA), Caco-2 permeability, LogP, blood–brain barrier penetration (BBB), and plasma protein binding (PPB), which are shown in **(Table-5. 2)**

Table 5. 2 Virtual pharmacokinetic screening of compounds AC1–AC8

Cmds	Caco-2 Permeability	HIA	F(20%)	F(30%)	LogP	BBB	PPB	Lipinski rule violations	Acceptance
AC1	-4.796	0.106	0.005	0.994	6.391	0	81.12%	1	Accepted
AC2	-4.976	0.425	0.1	1	5.711	0.001	90.22%	1	Accepted
AC3	-4.756	0.004	0.01	0.233	7.663	0.84	98.31%	1	Accepted
AC4	-5.74	0.071	0.005	0.897	1.187	0.399	53.42%	0	Accepted
AC5	-5.099	0.428	0.04	1	6.594	0	94.08%	1	Accepted
AC6	-4.882	0.145	0.026	0.999	6.12	0	88.70%	1	Accepted
AC7	-4.807	0.081	0.006	0.992	6.418	0	83.43%	1	Accepted
AC8	-525	0.741	0.985	1	5.945	0.001	97.41%	2	Rejected

Note: Lipinski's rule states that an orally active drug has no more than one violation out of the five rules. A dru more than one rule can be rejected from the study.

5.2.5 Network pharmacology

5.2.5.1 Prediction of compound and disease targets

Approximately 100 genes were predicted for each compound using SwissTargetPrediction, while the SEA database provided information on 50–80 genes, and bindingDB yielded data on 30–40 genes. For AC4, 446 genes were identified from Gene Cards. Upon combining genes from all sources for each compound, the totals were as follows: 179, 161, 185, 532, 207, 145, and 150 for compounds AC1, AC2, AC3, AC4, AC5, AC6, and AC7, respectively. These genes were cross-referenced with cancer target genes obtained from GeneCards and DisGeNet individually, Common genes were further analyzed based on centrality parameters such as betweenness, closeness, degree, eigenvector, and local average

connectivity. The CytoNCA program was used to screen the top 20 genes based on node degree.

5.2.5.2 Compound-gene pathway network

All enrichment terms were thoroughly investigated, and pathway information for the genes was accessed from ShinyGO. A Compound-Gene- Pathway network was constructed in Cytoscape, illustrating nodes in three tiers connected by multiple edges **(Figure 5.19)**. The network consists of 98 nodes connected by 227 edges, with an average number of neighbours of 4.633and a characteristic path length of 3.123. Analysis data indicates network density, heterogeneity, and centralization values of 0.048, 1.172, and 0.183, respectively.

Apart from the pathway for gastric cancer, many compounds were found to interact in numerous otherpathways such as epithelial cell signaling in *Helicobactor pylori* infection, natural killer cell-mediated cytotoxicity, Epstein–Barr virus infection, colorectal cancer, pancreatic cancer, small cell lung cancer, non-small cell lung cancer, prostate cancer, and breast cancer. It was evident that *H. pylori* infection can activate various pathways including MAPK, NF-κB, Ras, PI3K, and STAT3, which can trigger cellular mechanisms such as proliferation, differentiation, apoptosis, or cell migration [188]. Overexpression of EGFR and HER2 plays a significant role in the carcinogenesis of gastric, endometrial, ovarian, lung, breast, and urinary bladder cells [123].

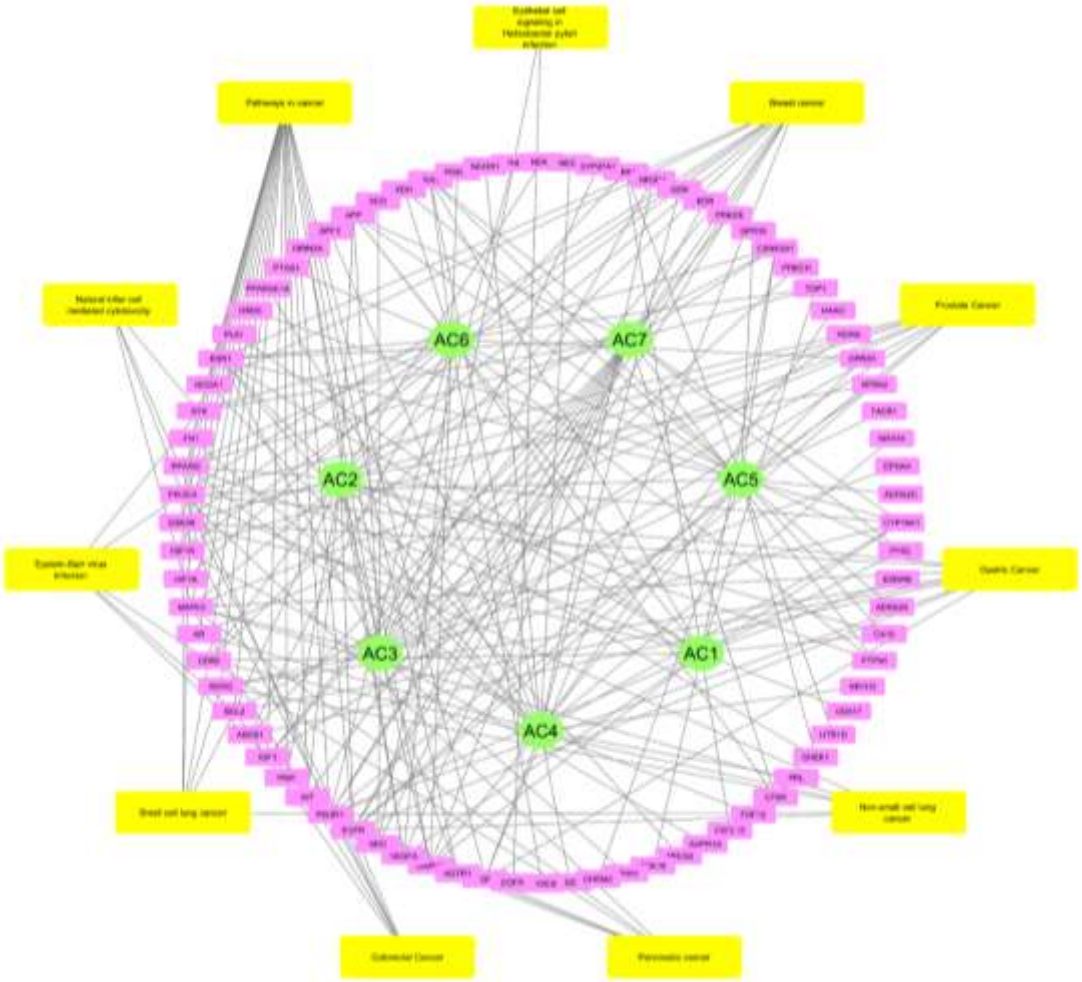

Figure 5. 19 Compound-gene-pathway network of compounds AC1–AC7

Table 5.3: Enrichment values of all the pathways (AC1-AC7)

Pathways	**Total genes**	**Pathway genes**	**Enrichment FDR**	**Fold Enrichment**
Pathways in cancer	22	530	1.19E-16	13.0106
Breast cancer	12	147	2.07E-12	25.5868
Prostate cancer	9	97	3.94E-10	29.0819
Gastric cancer	9	148	1.01E-08	19.0604
Non-small cell lung cancer	6	72	6.89E-07	26.1198
Pancreatic cancer	6	76	8.75E-07	24.745 1
Colorectal cancer	6	86	1.61E-06	21.8677
Small cell lung cancer	6	92	2.10E-06	20.4416
Epstein-Barr virus infection	5	202	0.0009	7.7583
Natural killer cell mediated cytotoxicity	4	130	0.0015	9.6442
Epithelial cell signaling in Helicobacter pylori infection	2	70	0.0304	8.9553

5.2.5.3 Hierarchical network and synergy

The reconstruction of the hierarchical network for the gastric cancer pathway from the three-tier network suggests that many genes are targeted by more than one compound, indicating the potential for combination synergy. In the hierarchical network for gastric cancer (**Figure 5.20**), the gene EGFR can be targeted by AC2, AC5, and AC7. Similarly, PIK3R1 is targeted by AC1, AC6, and AC7, while ABCB1 is targeted by both AC6 and AC7. GSK3B is targeted by AC1 and AC2. These interactions have the potential to produce synergy. EGFR was found to activate ERK/MAPK, phosphatidyl-inositol-3-kinase (PI3K), JAK/ STAT pathway, and the downstream effectors to regulate cell proliferation, migration, and tumour angiogenesis. EGFR is highly expressed in gastric cancer. Out of 78 positive cases of gastric cancer, 57.7% of patients were found with expressed EGFR [189]. Reported that miR-221-3p probably helps in promoting tumors in gastric cancer by negatively regulating PIK3R1 expressions, thus PIK3R1 was reported as a target in gastric cancer therapy demonstrated that GSK3B is one of the downstream effectors of ILK upon FGFR inhibition [110, 190], and targeting ILK would enhance the effectiveness of AZD4547 treatment of gastric tumors [110]. Other genes such as PIK3CA, MAPK3, BCL2, FGF9, and RXRG are shown to interact with a single compound only.

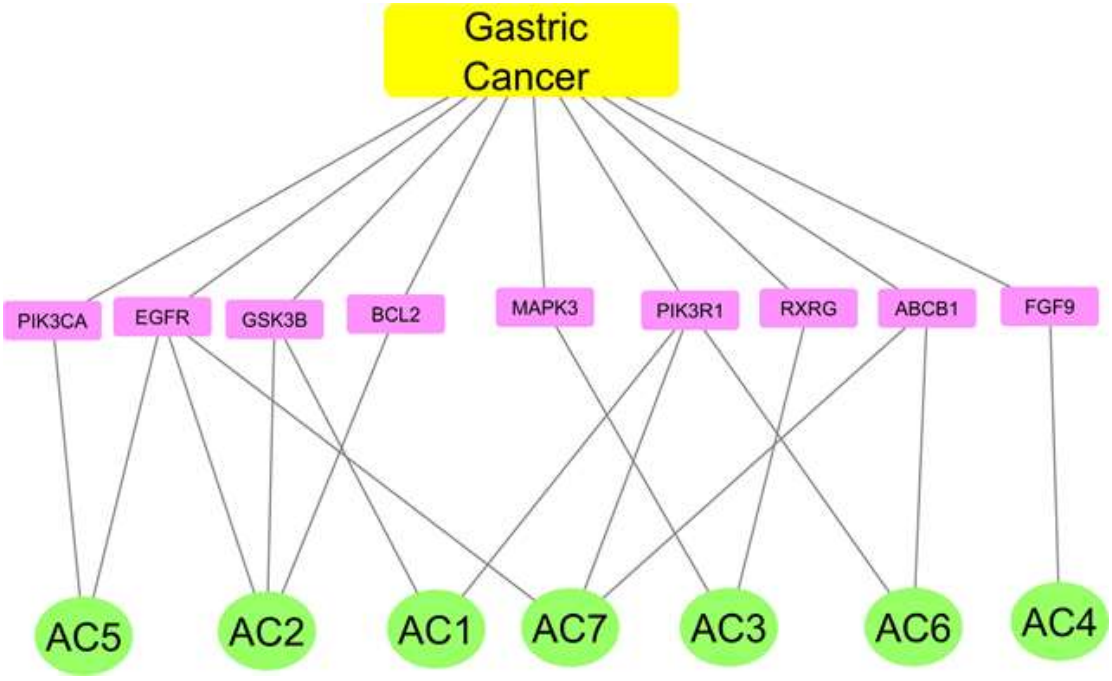

Figure 5. 20 Hierarchical networks for gastric cancer

5.2.5.4 Protein–protein interactions

The analysis of protein–protein interactions (PPI) was conducted by constructing a protein–protein network using STRING, including all the screened top genes. The construction was performed at the highest confidence level of 0.9, and all disconnected nodes were hidden from the network. A total of 79 nodes were found, interacting via 83 edges, which is considerably higher than the expected number of edges (22), indicating a significantly higher level of interactions. The average node degree is the enrichment P-value was found to be less than 1.0e-16. Furthermore, the network was clustered using a k-means (obsolete) style with five clusters. The protein–protein network is shown in **Figure 5.21**. Genes like EGFR, ESR1, IGF1R, KDR, NCOA1, NCOR1, PIK3CA, PIK3R1, and SRC forms the hub proteins, among which EGFR, ESR1, and SRC shows the high node degree of 11, 16, and 14 respectively. Cluster 1 nodes shown in red contains 18 nodes (AGTR1, AHR,

APP, CDK18, CHRM2, EPHA1, FGF12, NCOA1, NCOR1, NR1H3, NR1H4, NR3C1, NTRK2, OPRD1, PPARG, PPARGC1A, PRKCH, and XDH), cluster 2 in yellow also contains 17 nodes (ABCG2, ADRA2C, BCL2, CDK17, CDK6, CHEK1, CTSK, DAPK1, DRD5, EPHA4, GSK3B, GSN, HIF1A, MAPK3, NEK6, PIM1, and PRKCE), cluster 3 in green contains 17 nodes (ABCB1, ADRA2A, CA10, CYP19A1, CYP27A1, DPF3, GPR35, HAAO, PDE5A, PLK1, PYGL, RGS6, RORA, RXRG, SCD, TACR1, and VRK2), cluster 4 in cyan contains 17 nodes (AR, AVPR1A, CSNK2A1, EGFR, EPHB2, ESR1, FN1, GRIN2A, IGF1R, MED1, PIK3CA, PIK3CG, PIK3R1, PTGS1, PTPN1, SRC, SYK), and cluster 5 in blue includes 10 nodes (CXCL12, EDNRB, FGF9, HTR1D, IGF1, KDR, KIT, PRL, TOP1, and VEGFA). The average local clustering coefficient is 0.299.

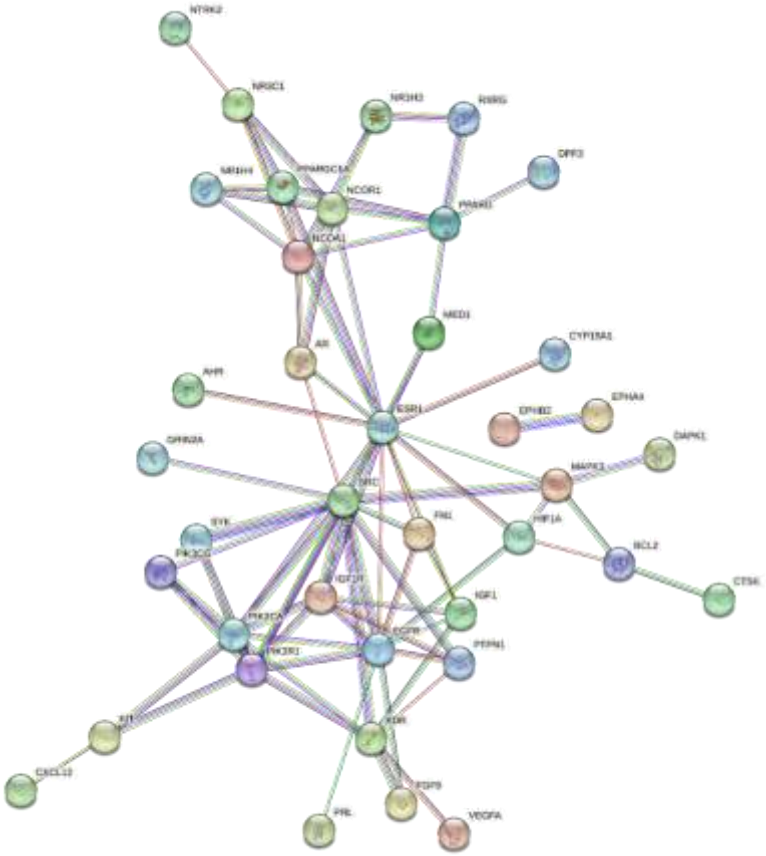

Figure 5. 21 Protein-protein networks for AC compounds genes

5.2.5.5 KEGG pathway and gene ontology(GO)

In ShinyGO, the KEGG pathway for gastric cancer **(Figure 5.22)** was analysed for all the genes associated with the compounds. Genes such as GSK-3β, EGFR, PI3K, ERK1/2, BCL2, FGF, MDR1, and RXR are highlighted in red, matching the input genes. Specifically, GSK3B is targeted by AC1 and AC2, EGFR by AC2, AC5, and AC7, and PIK3R1 by AC1, AC6, and AC7. Additionally, BCL2 is targeted by AC2, FGF by AC4, and RXR by AC3. Furthermore, GO analysis provides insights into the most relevant biological processes, cellular components, and molecular functions of the hub genes under study. The GO data for the top 20 biological processes, cellular components, and molecular functions are illustrated respectively, in the form of bar plots, where the bars represent the fold enrichment. “Response to organic cyclic compound” was found to be the top biological process down regulated by the genes, and the prominent cellular component was “phosphatidyl 3-kinase complex class IA.” Additionally, the most important molecular function related to the compound genes is “nuclear receptor activity.”

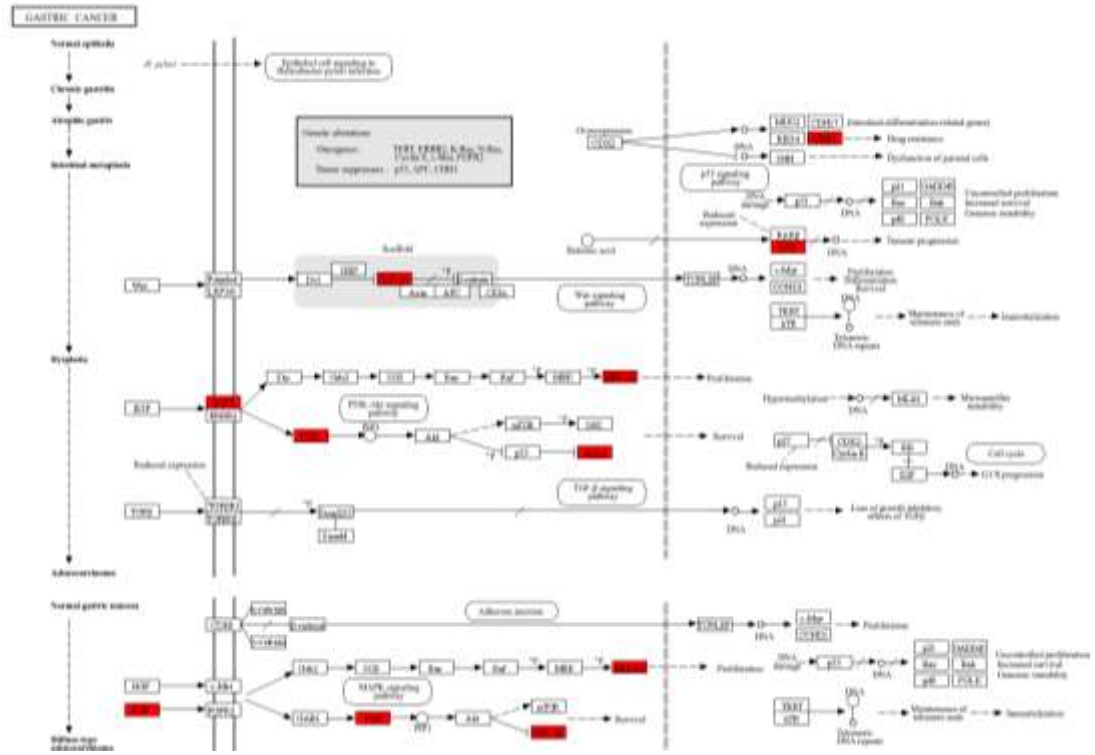

Figure 5. 22 KEGG pathway for all the genes associated with the compounds AC1–AC7

5.2.6 Computational studies

5.2.6.1 Molecular docking studies of compounds with EGFR, PIK3R1 AND GSK3B

The interaction capacity of ligands with proteins was assessed by calculating the binding energy, where lower energy indicates greater stability in ligand conformation upon binding to the protein. A ligand with a binding affinity equal to or lower than −7 Kcal/mol is considered to meet the criterion for valid molecular binding. For this study, the molecular docking studies indicate that all compounds exhibited high-level binding potentials. Visual analysis of the binding sites of the selected conformers of EGFR, PIK3R1, and GSK3B was conducted using BIOVIA Discovery Studio 2024 software, and the results are provided in **Table-5.4** respectively. Furthermore, a visual examination of the 2D structures revealed that the ligand AC6 binds with PIK3R1

receptor through four hydrogen bonds with ARG-365, THR-366, and ARG-417 residues.

Table 5.4 Binding affinity (kcal/mol) of the selected compounds with EGFR, PIK3R1and GSK3B proteins

Proteins	Grid coordinates	Grid size	Compounds	Binding affinity (kcal/mol)
EGFR	22.01, 0.25, 52.79	19 × 19 × 19	AC2	−7
			AC5	−9.4
			AC7	-9.7
PIK3R1	−5.82, 23.15, −17.31	30 × 30 × 30	AC1	−7.7
			AC6	−8.4
			AC-7	-8.4
GSK3B	37.83, 35.43, 55.75	16 × 16 × 16	AC1	−8
			AC2	−8.1

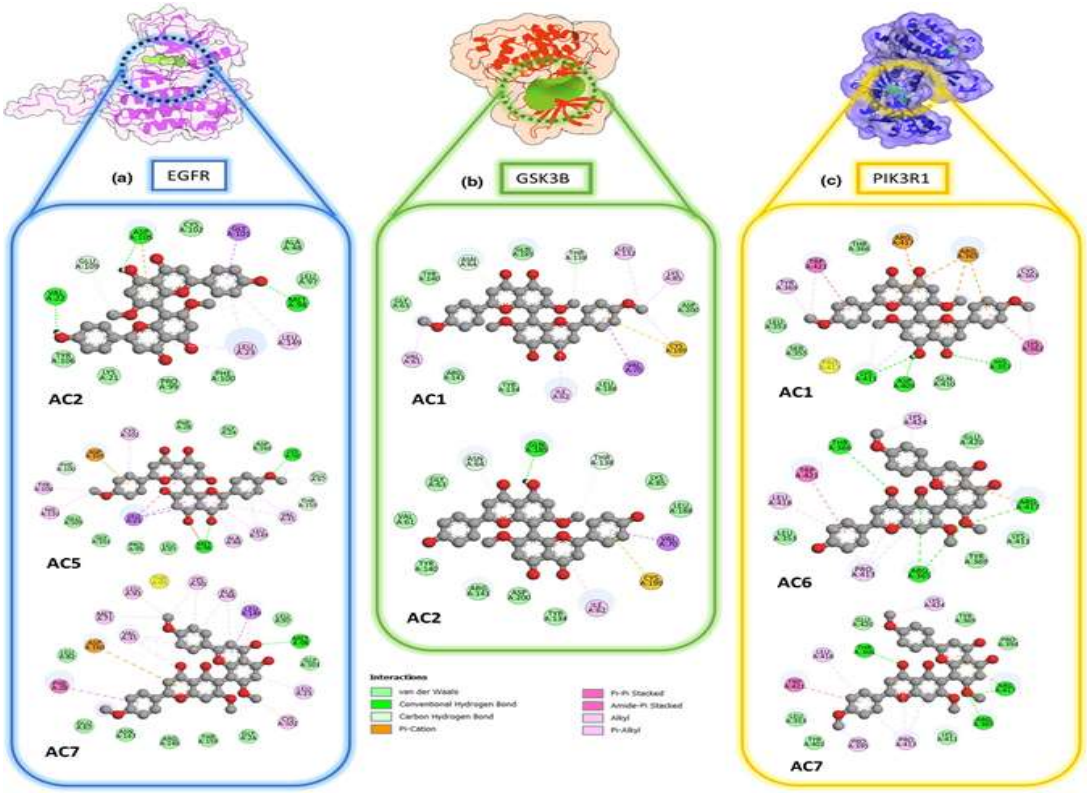

Figure 5. 23 2D docked conformers of EGFR, GSK3B, and PIK3R1 with their respective ligands.

5.2.6.2 Molecular dynamics simulation studies

Ligand-protein interaction of Compound AC2 and AC5 against GSK3β and EGFR protein respectively

We selected AC2 and AC5 for MD simulations based on docking and network pharmacology studies. The analysis of trajectories obtained from the MD simulation studies of AC2 with GSK3β protein depicted slight fluctuation complex between 20 ns and 30 ns time scale **(Figure-5.24)**. After that, the complex fairly stabilized throughout the course of the simulation time scale. The average RMSD of the complex was at around 0.55 nm, and the maximum deviation was found to be 0.6 nm at around 25 ns. Ligand was quite stable throughout the simulation, with an average RMSD of 0.6 nm. The RMSF plot of the protein revealed a higher number of fluctuations at residues between 40 and 50 positions, which are away from the residues involved in hydrogen bonding with the ligand. So, the protein backbone was quite stable during the simulation run. To assess the ligand conformational stability in the binding pocket of the receptor, we have evaluated the RMSF of the ligand. with an RMS fluctuation of 0.15 and 0.2, respectively. Fluctuation found in the ligand indicates that small molecular structure of the ligand was trying to stabilize in the binding pocket of the protein. To evaluate the folding and unfolding of protein molecule during the simulation we have calculated radius of gyration value. The average Rg value was found to be 2.25 nm, and the highest deviation was at 50000 ps time scale. Solvent accessible surface area (SASA) is a measure of surface area of protein available to ligand molecule. SASA can help to analyse the structural changes of the protein upon ligand binding. The average SASA of protein–ligand complex during the simulation run was calculated and found to be 200 nm^2. To analyses the protein conformational stability and flexibility, we also

evaluated Principal Component Analysis (PCA). The covariance trace value of complex was found to be 40 nm. The ligand binding affected the overall motion of the protein in conformational space. All these results suggest that at the initial stage, the ligand was finding its most favourable binding state as the simulation run progressed, the ligand was found quite stabilized in the binding pocket.

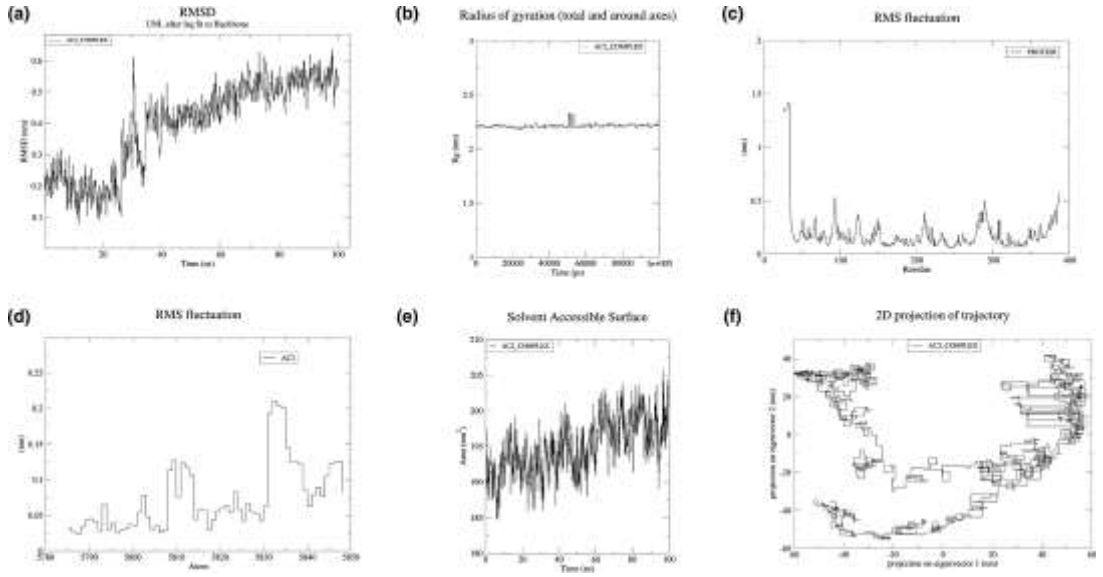

Figure 5.24 MD simulation of compound AC2 and GSK3β protein. (a) RMSD of AC2–GSK3β complex, (b) Rg of AC2–GSK3β complex, (c) RMSF of GSK3β, (d) RMSF of AC2, (e) SASA of AC2–GSK3β complex, and (f) PCA of AC2–GSK3β complex

Furthermore, the MD simulation data of ligand AC5 and EGFR protein did not reveal much fluctuation in the complex system during the simulation run. However, a slight fluctuation was found at 30 ns time scale (**Figure-5.25**). The average RMSD calculated was 2.25 nm. The RMSF plot depicted slight fluctuation at 850–900 residues. These residues were not involved in hydrogen bonding with the ligand. So, it will not affect the conformational stability of the complex molecule. Average RMSF of protein found was 0.4 nm. RMSF plot of ligand showed quite a fluctuation throughout the simulation run, which depicted ligand was adjusting to its most stable conformation in the binding pocket of the receptor. Radius of gyration shows

quite stability throughout the simulation and average value found to be 2 nm. SASA plot depicted that there was quite destability during the 0–20 ns time scale. After that, it was quite stabilized at around 80 ns time scale. The covariance trace value from the PCA analysis of the complex was found to be 20 nm, which suggests that ligand binding results in a slight change in the overall motion of protein from its clusters in conformational space [191]. All these results suggest that the ligand was quite stable throughout the course of a simulation run.

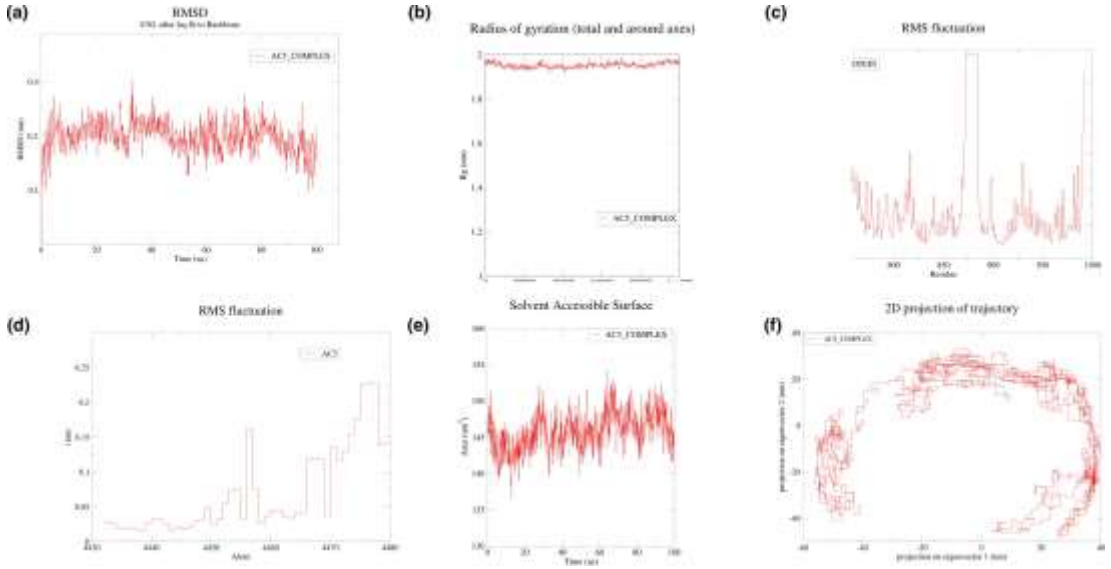

Figure 5.25 MD simulation of compound AC5 and EGFR protein. (a) RMSD of AC5–EGFR complex, (b) Rg of AC5–EGFR complex, (c) RMSF of EGFR, (d) RMSF of AC5, (e) SASA AC5–EGFR complex, and (f) PCA of AC5–EGFR complex

5.2.7 Biological activity of compounds

5.2.7.1 MTT assay for gastric cancer

The isolated compounds **AC1**, **AC2**, and **AC5** were evaluated for in vitro cytotoxic activity against human gastric adenocarcinoma, The Crude was tested on several cell lines among them AGS shown more significates hence we designed the study on this cell lines by MTT assay. As described in the materials and methods section, the cells were treated with different concentrations (3.125, 6.25, 12.5, 25, 50, and

100 μM) of AC1, AC2, and AC5, and apigenin. In this study, a dose-dependent cytotoxicity of these compounds was evaluated, where the effects of varying concentration on the percentage survival rate of the cells were observed after 24 h. The untreated cells were found to be healthy after the same period of time. The half-maximal inhibitory concentration (IC_{50}) for compounds AC1, AC2, AC5, and apigenin were found to be 90.58, 119.8, 107.8, and 174.5μM, respectively. % Survival versus concentration (μM) curves for all four compounds are given in **Figure 5.26**

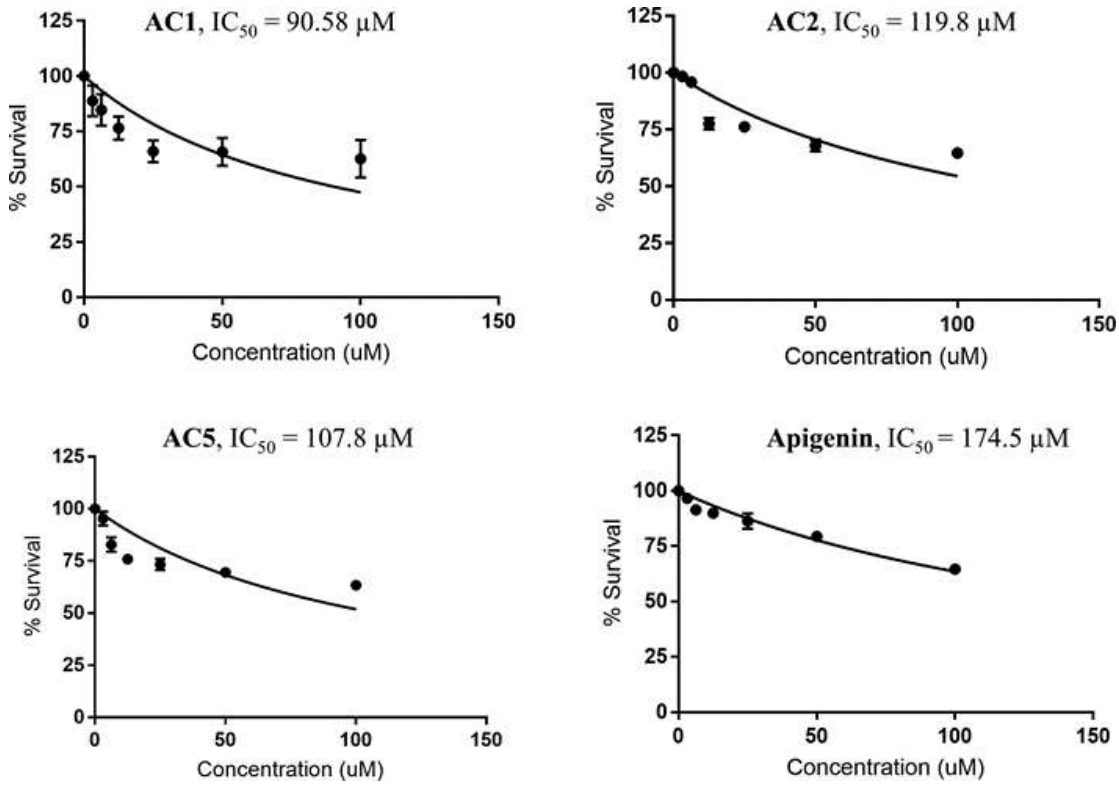

Figure 5. 26 Concentration versus % survival curves for compounds **AC1, AC2, AC5**, and apigenin in MTT assay on AGS Cell line.

5.3 Experimental section

5.3.1 General Experimental Procedures

All the chemicals were purchased from Sigma-Aldrich, which were used exactly as received. Pre-coated silica gel-60 GF-254 aluminum sheets (Merck) were used for

TLC, and the spots were visualized under UV light at 254 and 366 nm. One-dimensional and two-dimensional NMR spectra were recorded on 500 and 600 MHz instruments. The chemical shifts (ppm) of protons and carbons are reported chemically downfield from tetramethylsilane (TMS), with the leftover proton/carbon in the NMR solvent ($CDCl_3$, 7.26/77.1 ppm; DMSO-d6, 2.50/39.5 ppm; MeOD, 3.32/49.0 ppm) serving as a reference. Agilent 1100 LC-QTOF and HRMS-6540-UHD instruments were used to record ESI-MS and HRMS spectra. Utilizing an Agilent Triple-Quad LC-MS/MS system (model 6410), LC- ESI-MS/MS analysis was performed.

5.3.2 Plant material

The plant material, *A. cunninghamii*, was collected and authenticated by Dr. Bikarma Singh, Scientist on 07 August 2019, from the Jammu region of India. A specimen sample (accession number, 24176) was preserved in Janaki Ammal Herbarium at the CSIR-Indian Institute of Integrative Medicine, Jammu, India. Presently he is working as Senior scientist CSIR-National Botanical Research Institute, Lucknow, India.

5.3.3 Preparation of the extract

Coarsely powdered leaves (1 kg) were extracted three times at room temperature using overhead stirring for 3 h per cycle using (3 L) methanol. Clear organic layer was obtained by filtering that was concentrated by evaporating the solvent using a rotary evaporator to obtain a viscous crude extract (220 g; 22% extractive value). The extract was subjected to LC-MS analysis and database mining for the identification of metabolites. Further, chromatographic purification was performed on the sample to

isolate the identified metabolites.

5.3.4 LC-HRMS and database mining

The 10 mg of the extract was dissolved in LC-MS grade methanol (10 mL) and subsequently filtered through a 0.25-micron filter. One microliter of this solution was injected into the LC-MS system. LC-MS analysis was done using the UPLC system, equipped with Agilent 6540 Ultra High Definition (UHD) QTOF LC/MS system, and BEH C18 column (1.7μm, 2.1 × 100 mm). The separation was performed at a flow rate of 10 uL/min, where the mobile phase used for liquid chromatography was acetonitrile to 0.1% (v/v) formic acid in water (65:35). The run time was 15 min. The LC-HRMS data were acquired in ESI positive, with MS acquiring parameters as follows: capillary voltage, 4000 V; drying gas temperature, 300°C; drying gas flow, 8 L/min; nebulizing pressure, 35 psi. The scan source parameters, capillary voltage, skimmer voltage, and fragmentor voltage were 4000 V, 65 V, and 150 V, respectively. DNP was utilized for data mining and compound identification that was accessible through CHEMnetBASE at https://dnp.chemnetbase.com/.

5.3.5 Chromatographic purification and characterization of the secondary metabolites

Fifty grams of the extract was loaded onto a silica gel column and fractionated using gradient elution with increasing concentrations of ethyl acetate in hexane. Five fractions were collected: fr 1 (10% ethyl acetate, 7 gm), fr 2 (30% ethyl acetate, 2.5 gm), fr 3 (50% ethyl acetate, 5 gm), fr 4 (75% ethyl acetate, 11 gm), and fr 5 (100% ethyl acetate, 4 gm). These fractions were screened for cytotoxicityand the highest cytotoxicity was observed for the fraction 2. The fraction 2 was further

subjected to repeated chromatography for the purification of compounds. The silica gel column was monitored by TLC under UV-254 nm. The fractions were pooled together based on the TLC profile. Semi-pure fractions were further purified over Sephadex LH-20 and HPLC. A total of seven compounds were purified and characterized based on the spectral properties. Among them four compounds were characterised as biflavones; cupresuflavone; 4′,4″,7,7″ tetra-methoxy or WB1 (**AC1**), cupresuflavone; 7,7″-dimethoxy (**AC2**), and cupresuflavone; 4′,4″-dimethoxy or W11 (**AC5**). Apart from the targeted biflavones **AC1**, **AC2**, and **AC5**, a cupressuflavone; 4′,7,7″-trimethoxy (minor amount) was also obtained. This compound was considered neither for network pharmacology nor for *in-vitro* studies due to its limited yield. This is the first report of its isolation and identification (a previously undescribed compound). Other isolates were characterized as abietic acid (major constituent of this species), β-sitosterol, (**AC3**, a very common plant metabolism) it is a crystalline substance was obtained during the early phase of extract preparation while concentrating separating by filter paper and later characterised as phthalic acid **(AC4).**

Abietic acid: White solid; 15 mg; ^{1}H-NMR (500 MHz, $CDCl_3$) δ 5.77 (s, 1H),5.37 (s, 1H), 2.22 (m, 1H), 2.11–2.03 (m, 4H), 1.96 (s, 1H), 1.88 (d, 2H), 1.84–1.75 (m, 3H), 1.68 (s, 1H), 1.66 (s, 1H), 1.62–1.54 (m, 3H), 1.25 (s, 3H), 1.01 (dd, 6H), 0.83 (s, 3H). ^{13}C-NMR (125 MHz, $CDCl_3$) δ 184.96, 145.28, 135.57, 122.39, 120.49, 50.94, 46.34, 44.90, 38.27, 37.18, 34.88, 34.46, 27.45, 25.61, 22.47, 21.41, 20.87, 18.05, 16.71, 14.03. HRMS *m/z* 303.2319 $[M+H]^+$ (calcd for $C_{20}H_{31}O_2^+$, 303.2319)[119].

Cuppresuflavone: 4′,4″,7,7″ tetra-methoxy or WB1 (AC1): White solid; 10 mg; ^{1}H-NMR (500 MHz, CDCl3) δ 13.21 (s, 2H), 7.43 (d, J = 8.9 Hz, 4H), 6.86 (d, J =

9.0 Hz, 4H), 6.59 (d, J = 5.1 Hz, 4H), 3.82 (s, 6H), 3.80 (s, 6H). ^{13}C-NMR (125 MHz, CDCl3) δ 182.96, 163.95, 163.33, 162.64, 162.61, 154.65, 127.62, 123.25, 114.57, 105.28, 103.51, 99.47, 95.30, 56.27, 55.52. HRMS m/z 595.1585 $[M+H]^+$ (calcd for $C_{34}H_{27}O_{10}^+$, 595.1599)[192].

Cuppresuflavone: 7,7″-dimethoxy (AC2): White solid; 9 mg; ^{1}H- NMR (600 MHz, DMSO) δ 13.27 (s, 1H), 12.96 (s, 1H), 7.98 (d, *J* = 8.8 Hz, 1H), 7.56 (d, *J* = 8.7 Hz, 1H), 7.38 (d, *J* = 8.6 Hz, 2H), 6.94–6.85 (m, 4H), 6.81 (s, 1H), 6.79 (s, 1H), 6.69 (m, 4H), 3.73 (s, 6H). ^{13}C-NMR (150 MHz, $CDCl_3$) δ 183.02, 164.71, 163.33, 162.29, 154.56, 128.30, 127.83, 115.96, 114.39, 104.98, 104.96, 102.64, 95.19, 56.19. HRMS *m/z* 567.1274 $[M+H]^+$ (calcd for $C_{32}H_{23}O_{10}^+$, 567.1286).

***β*-sitosterol (AC3):** White solid; 7 mg; ^{1}H-NMR (500 MHz, $CDCl_3$) δ 5.39–5.31 (1 H, m), 3.52 (1 H, ddd), 2.42–2.13 (2 H, m), 1.98 (2 H, t dd), 1.89–1.77 (3 H, m), 1.74–1.38 (11 H, m), 1.33–1.22 (5 H, m), 1.21–1.03 (6 H, m), 1.03–0.96 (4 H, m), 0.93 (4 H, t), 0.87–0.74 (8 H, m), 0.75–0.64 (3 H, m). ^{13}C-NMR (125 MHz, $CDCl_3$) δ 140.93, 121.88, 71.98, 56.93, 56.22, 50.30, 46.01, 42.47, 39.94, 37.42, 36.67, 36.31, 34.11, 32.07, 31.84, 29.86, 29.32, 28.40, 26.25, 24.46, 23.23, 21.25, 19.97, 19.55, 19.19, 18.94, 12.14, 12.02. HRMS *m/z* 415.2296 $[M+H]^+$ (calcd for $C_{29}H_{51}O^+$,415.3934)[187]

Phthalate (AC4): White solid; 10 mg; ^{1}H-NMR (600 MHz, $CDCl_3$): δ 7.72 (m, 2H), 7.56–7.50 (m, 2H), 4.09 (q, 4H), 0.99 (t, 6H). ^{13}C-NMR (150 MHz, $CDCl_3$) δ 167.70, 132.39, 130.93, 128.86, 71.81, 19.17

Cuppresuflavone: 4′,4″-dimethoxy or W11 (AC5): White solid; 10 mg; ^{1}H-NMR (600 MHz, MeOD) δ 7.80 (s, 2H), 7.31 (d, *J* = 8.8 Hz,4H), 6.64 (d, *J* = 8.8 Hz, 4H), 6.59

(s, 2H), 6.54 (s, 2H), 3.73(s, 6H). ^{13}C- NMR (150 MHz, MeOD) δ 182.18, 163.99, 162.91, 161.48, 160.60, 153.69, 126.82, 120.62, 114.71, 103.55, 101.13, 98.75, 94.10, 77.23, 54.71. HRMS *m/z* 567.1274[M+H]$^+$(calcd for $C_{32}H_{23}O_{10}^+$, 567.1286)[192]

Cupressuflavone: 4′,7,7″-Tri-Methoxy: White solid; 3mg; ^{1}H-NMR (600 MHz, CDCl3) δ 13.19 (s, 1H), 13.05 (s, 1H), 7.41 (dd, J = 21.2, 8.4 Hz, 4H) 6.85 (d, J = 8.4 Hz, 4H), 6.63–6.56 (m, 4H), 3.80 (m, 9H). ^{13}C-NMR (150 MHz, CDCl3) δ 182.92, 182.85, 164.18, 164.06, 163.49, 163.29, 162.68, 162.60, 162.51, 159.87, 154.61,154.59, 127.82, 127.63, 123.00, 122.74, 116.03, 114.44, 105.09, 105.02, 103.13, 103.10, 99.53, 99.34, 95.28, 95.13, 56.30, 56.25, 55.48 HRMS m/z 581.1406 [M+H]$^+$ (calcd for $C_{33}H_{25}O_{10}$, 581.1442).

5.3.6 Virtual ADME analysis

All the selected compounds were subjected to pharmacokinetic analysis by *in-silico* method. In ADMETlab2.0 (https://admetmesh.scbdd.com/service/ screening/cal), parameters like bioavailability ($F_{20\%}$, $F_{30\%}$), human intestinal absorption (HIA), and Caco-2 permeability were evaluated. All the favourable compounds were again screened based on Lipinski's rule of 5 using Swiss ADME (http://www.swissadme.ch). Compounds violating more than one rule were rejected[193].

5.3.7 Network pharmacology

Drug target databases, SwissTargetPrediction (http:// www.swisstargetprediction.ch) [194],BindingDB(https://www.bindingdb.org/rwd/bind/chemsearch/marvin/FMCT.js

p)[114], and SEA database (https://sea.bkslab.org/) were searched using the canonical SMILES of the compounds as input. Similarly, gene targets to cancer were also obtained from the web sources like GeneCards (https://www.genecards.org/) and DisgeneNet (https://www.dis-genet.org/search). Results obtained for each compound from all the sources were combined and compared with the disease genes individually by using Venn diagram (https://bioinformatics. psb.ugent.be/webtools/Venn/). From the common genes, top 20 genes for each compound were identified based on degree parameters by the use of CytoNCA program [195].

Top 20 genes were used for enrichment analysis in ShinyGo (http:// bioinformatics.sdstate.edu/go/), and all the prominent related pathway information were gathered. A three-tier network was constructed where the outer nodes were the pathways, middle nodes indicate the genes, and the core nodes refer to the compound codes. This layout was prepared in Cytoscape (version 3.10.1) by merging pathway-gene network and compound-gene network and then analyzed [195].

All the top genes under study were subjected to STRING (https://string-db.org/) for investigation of the interactions between them. Providing the list of genes in multipleprotein columns and using the filter for *Homo sapiens*, thestring network was constructed. The highest topology, the networks were analyzed, and the common genes targeted by different compounds were studied that showed synergy

KEGG pathways were analyzed for the selected genes where matched genes were highlighted in red. This study was done in ShinyGO (http://bioinformatics.sdstate. edu/go/). Setting *Homos sapiens* as the species and the FDR cutoff 0.05, top 20

pathways were evaluated. Gene Ontology data for biological processes, cellular components, and molecular functions were studied and all the chart plots were downloaded[110].

5.3.8 Prediction of the known targets

Drug target databases, SwissTargetPrediction (http://www.swisstargetprediction.ch) [194], BindingDB (https://www.bindingdb.org/rwd/bind/) [196], and SEA database (https://sea.bkslab.org/) were searched using the canonical SMILES of the compounds as input. Similarly, gene targets related to cancer were also obtained from the web sources like Gene Cards (https://www.genecards.org/) and DisgeneNet (https://www.disgenet.org/search). Results obtained for each compound from all the sources were combined and compared with the disease genes in dividually by using Venn diagram (https://bioinformatics. psb.ugent.be/webtools/Venn/). From the common genes, top 20 genes for each compound were identified based on degree parameters by the use of CytoNCA program [197].

5.3.9 Molecular docking

The canonical SMILES of ligands were retrieved from PubChem (https://pubchem.ncbi.nlm.nih.gov/), and 3D structures were generated using the Chem3D module of Chem Office Suite 2020 v20.1.1.125 software and saved in mol2 format. The crystal structures of proteins EGFR (PDB ID: 1M17), PIK3R1 (PDB ID: 5LKZ), and GSK3B (PDBID:3I4B) were retrieved from RCSB PDB (https://www.rcsb.org/). All the small molecule ligands, water molecules, and symmetry chains were removed from the proteins using BIOVIA Discovery Studio 2024 software. Further, the structures were saved in PDBQT formats after

processing the protein crystals by the addition of hydrogen, calculation of charges, and assignment of atomic type in AutoDockTools 1.5.7. Grid coordinates and grid sizes were detected for the docking region of proteins using Discovery Studio. The binding of the ligands to the corresponding proteins was verified by molecular docking, which was performed using the software AutoDock Vina 1.1.2–64 to obtained 10 different docked structures and affinity scores for each protein–ligand pair. Among them, one with the lowest binding energy was chosen and the docking pattern was visualized in Discovery Studio software.

5.3.10 Molecular dynamics simulation studies

To further understand the binding stability and conformational changes of the top identified compounds in the irrespective targets, full atom-based MD simulation using the GROMACS 2020 version was employed on Param Shivay HPC (IIT BHU). The docked conformations were used as a starting point for the simulation. The input files for MD simulation were generated via the CHARMM GUI (https://charmm-gui.org/). The TIP3P water model was utilized to accommodate the water model in a rectangular box, and the distance between the protein complex and the box's edges was set to 10 Å. The system was neutralized to physiological pH 7.4 by the addition of the proper number of counter ions (Na^+ and Cl^- ions) at 0.15 M concentration. The prepared system was subjected to energy minimization (steepest descent algorithm), equilibration at NVT (Noose Hoover thermostat) and NPT (Berendsen thermostat) ensemble for a duration of 100 ps each. The final production step was carried out at 300.15 K and at 1 atm pressure for a duration of 100 ns with time step of 2 fs. Trajectory analysis involved the examination of generated trajectories through metrics

such as root mean square deviation (RMSD), root mean square fluctuation (RMSF), as well as the generation of plots for radius of gyration, solvent accessible surface area (SASA), and principal component analysis of eigenvectors. These plots were created using the XMgrace software package (GRACE v5.1.19) [198, 199].

5.3.11 *In-vitro* cytotoxicity study

For the cytotoxicity study, the MTT assay was conducted in triplicate using AGS cells (human gastric adenocarcinoma cell line), procured from NCCS, Pune, India. Cells were cultured in Dulbecco's modified Eagle medium (DMEM) (Gibco, USA) supplemented with 5% fetal bovine serum (FBS) (Gibco, USA) and 50 U/mL, 100 μg/mL, and 2 mM penicillin, streptomycin, and L-glutamine (Gibco, USA), respectively. The cells were incubated in 37°C and 5% CO2. Counting of the cells was done by trypan blue method and the cells were seeded on a 96-well culture plate with a density of 10,000 cells/well. DMSO was used as a positive control. The AGS cells were grown and treated with compounds AC1, apigenin, AC2, and AC5, in concentrations 3.125, 6.25, 12.5, 25, 50, and 100 μM. We used these compounds only because of high amount of concentration and based on docking studies. The culture was incubated for 24 h. Then the media was removed by washing the cells. A stock solution of MTT (3-(4,5-dimethylthiazol-2-yl)-2,5-diphenyltetrazolium bromide, a tetrazole) is reduced to purple formazan in living cells. Reagent was prepared (1 mg/mL) and diluted to 0.5 mg/mL solution. Fifty micro litter of MTT dye was added to all the cells and incubated in a CO2 incubator for 2.5 h. Cells were washed again and 100 μL of DMSO was added to each well, followed by shaking for 1.5 h. The cell viability was calculated by measuring optical density at 570 and 590 nm using an ELISA plate reader [200]